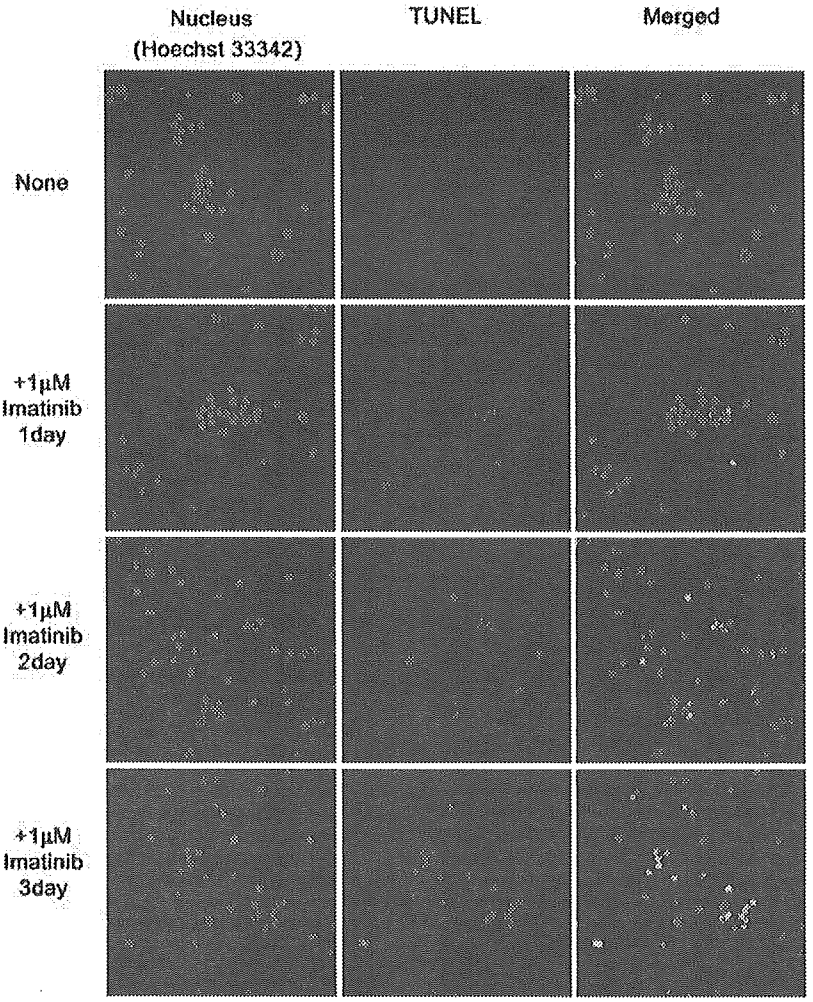

Figure 2 HeLa S3 is sensitive to a specific inhibitor of Abl, imatinib. HeLa S3 cells were treated with imatinib (1 μM), stained with Hoechst 33342 (2 μg/ml), and subjected to TUNEL assay at the indicated time points.

only the Rb-C phosphopeptide fragment surrounding Y805 has a sequence that adheres to a consensus sequence motif for Abl-catalysed phosphorylation (I/L/V–Y–X_{1-5}–P/F), as determined in a previous study (Figure 3c) (Cujec *et al.*, 2002).

In vitro kinase assays with [γ-^{32}P]ATP also demonstrated that Rb-C was phosphorylated via Abl, and the reaction was reversed by treatment with alkaline phosphatase (Figure 4a and data not shown). Studies using a series of point mutants of tyrosine residues within Rb-C showed that the Abl-catalysed phosphorylation reaction was significantly reduced in a Y805F mutant and was completely blocked in a Y771F/Y805F double mutant (Figure 4a). Thus, Abl phosphorylates Rb primarily at Y805 and partially at Y771.

Full-length Rb was phosphorylated *in vivo* by the Abl W118K mutant coexpressed in 293-T cells (Figure 4b), while the phosphorylation did not occur with the dominant-negative KD mutant (data not shown). To determine the sites of phosphorylation catalysed by the W118K mutant of Abl *in vivo*, we constructed Flag-tagged point mutants of Rb, in which Y771 or Y805 was replaced by phenylalanine. The Abl W118K mutant phosphorylated both wild-type Rb and the Y771F mutant to the same level, but phosphorylated the Y805F mutant much less efficiently even though the enzyme bound equally to the Rb mutants (Figure 4b). These results demonstrate that Abl phosphorylates Rb predominantly at Y805 both *in vivo* and *in vitro*, and suggest that Rb may be a downstream effector of Abl.

To further examine whether Rb was phosphorylated at Y805 endogenously within the cell, the phospho-Rb (Y805)-specific rabbit polyclonal antibody was raised against a synthetic phosphopeptide antigen including phosphoY805 (Materials and methods). The resulting antibody recognized Rb-C only when the protein was incubated with the constitutive active W118K mutant of Abl (Figure 5a). It also recognized the wild-type Rb and the Y771F mutant, but failed to detect the Y805F mutant, when the proteins were coexpressed with

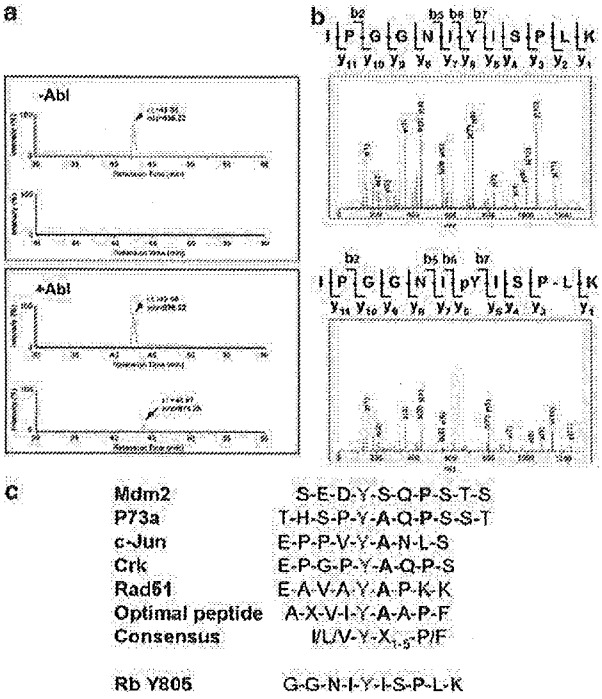

Figure 3 Tyrosine phosphorylation of Rb by Abl. (**a**) GST-Rb-C was incubated with (lower panel) or without (upper panel) a constitutively active mutant of Abl (W118K), separated by SDS–PAGE, digested with trypsin, and analysed by tandem MS. The MS spectra of peptides including Y805 (m/z = 636.22 and 676.25, indicated by arrowheads and an arrow, respectively) generated from tryptic digestion of GST-Rb-C are shown. (**b**) MS/MS spectra show that the amino-acid sequences of the peptides indicated by arrowheads and an arrow are IPGGNIYISPLK (upper panel) and IPGGNIpYISPLK (lower panel), respectively. (**c**) Sequence alignment of Abl phosphorylation sites. Amino acids indicated in bold are highly favored for phosphorylation by Abl (Cujec *et al*., 2002).

W118K in 293-T cells (Figure 5b), indicating that it was specific to the Y805-phosphorylated form of Rb. This antibody recognized endogenous Rb in K562 cells (Figure 5c), indicating that the protein carried a phosphorylated Y805. However, Rb became undetectable by the antibody after the cells were treated with imatinib, a potent inhibitor of Bcr/Abl, for 24 h (Figure 5c), whereas the activity of Bcr/Abl was completely inhibited (Figure 5d). Taken together, our results suggest that Bcr/Abl phosphorylates Rb at Y805 endogenously within K562 cells.

Ectopic expression of Rb induces apoptosis in tumor cells compromised by Abl-catalysed phosphorylation at Y805

It is known that the tyrosine kinase activity of Abl can be assessed by the extent of autophosphorylation. In fact, the W118K mutant of Abl was heavily phosphorylated when the mutant was expressed in the cell (Figure 4c). However, we noted that the W118K mutant recovered by coimmunoprecipitation with Rb was not detectable by the anti-phosphotyrosine antibody (Figure 4b), suggesting that Rb inhibited the kinase activity of Abl. Likewise, the tyrosine kinase activity of Abl appeared to be reduced significantly when the kinase was recovered from the cells that were coexpressed with Rb or its Y805F mutant (Figure 4c). Thus, our results suggest that excess Rb, as well as its Y805F mutant, binds and inhibits Abl tyrosine kinase activity.

Given that excess Rb inhibits Abl tyrosine kinase activity, we investigated the possible involvement of Rb in apoptosis of Abl-dependent tumor cells. Ectopic expression of GFP-tagged Rb induced the release of cytochrome *c* from mitochondria to the cytoplasm, condensation of nuclei, and DNA fragmentation in more than 50% of HeLa S3 cells (Figure 6a). Overexpression of Rb without GFP tag also induced apoptosis (data not shown). The Rb-induced apoptosis was also observed in the Abl-dependent CML cell lines (KU-812 and K562), but not in other tumor cell lines (MCF-7, A549, and 293-T cells; Figure 6b), suggesting that Rb induced apoptosis by inhibiting Abl tyrosine kinase activity. Consistent to this hypothesis, we found that coexpression of the constitutively active Abl W118K mutant could rescue cells from Rb-induced apoptosis, whereas the nonfunctional KD mutant had no effect (Figure 7a).

To examine the significance of Y805 phosphorylation in Rb-induced apoptosis, we prepared Y805F and Y805D Rb mutants in which the tyrosine residue was substituted by the neutral amino acid, phenylalanine, or by the acidic amino acid, aspartic acid, respectively, to mimic nonphosphorylated and phosphorylated forms of Rb. Ectopic expression of Y805F induced apoptosis at a level similar to wild-type Rb in HeLa S3 cells (Figure 7b). However, the Y805F-induced apoptosis was only partially suppressed by coexpression with W118K (Figure 7a and c, compare between Rb + W118K and Y805F + W118K). In contrast, the Y771F-induced apoptosis was suppressed by W118K at a level similar to wild-type Rb (Supplementary Figure 2). In addition, the apoptotic rate was partially suppressed when the Y805D mutant that mimicked a phosphorylated form of Rb was overexpressed within the cell, whereas Y771D was not effective (Figure 7b, c, and Supplementary Figure 2). Thus, our results suggest that Abl-catalysed phosphorylation of Rb at Y805 is necessary, but not sufficient, for survival of certain tumor cell types, including Bcr/Abl-positive CML.

Silencing of endogenous Rb by RNA interference (RNAi) induced apoptosis in Abl-dependent tumor cells

To further assess the involvement of Rb in survival of Abl-dependent human tumor cells, we prepared diced short interfering RNA (siRNA) of Rb and examined the effect of Rb silencing on the cells. Of three constructs designated as si-Rb-N, si-Rb-AB, and si-Rb-C (Materials and methods), si-Rb-N was most effectively suppressed the expression of GFP-Rb (Figure 8a). Transfection of this construct into K562 cells clearly showed that the silencing of endogenous Rb induced apoptosis, while the control lacZ si-RNA had marginal effect on the cell (Figure 8b). Thus, the result was consistent to

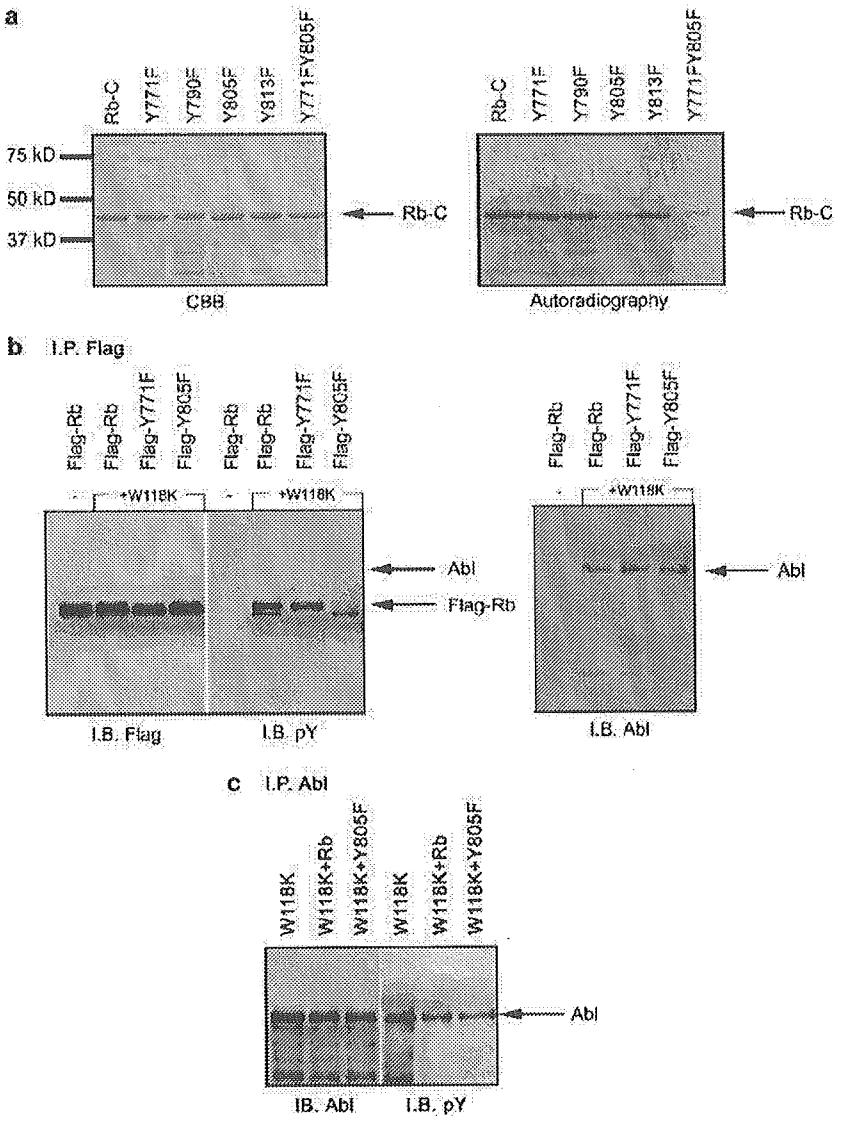

Figure 4 Rb Y805 is predominantly phosphorylated by Abl *in vitro* and *in vivo*. (**a**) *In vitro* kinase assays with [γ-^{32}P]ATP were performed on GST-Rb-C mutants, in which the indicated tyrosine residues in the C terminus were replaced with phenylalanine. Proteins were then separated by SDS–PAGE, followed by CBB staining (left panel) and autoradiography (right panel). (**b**) Flag-tagged Rb mutants in which Y771 or Y805 was replaced with phenylalanine were coexpressed with W118K in 293-T cells, followed by immunoprecipitation with anti-Flag and immunoblotting with anti-Flag (left panel), anti-phosphotyrosine (middle panel), or anti-Abl (right panel). (**c**) W118K were coexpressed with either the wild-type Rb or the Y805F mutant, followed by immunoprecipitation with anti-Abl and immunoblotting with anti-Abl (left panel) or anti-phosphotyrosine (right panel).

the experiments performed by using exogenously expressed Rb protein, and suggested that Rb plays a positive role in survival of Abl-dependent human tumor cells.

Discussion

Although Rb is known to be an upstream negative regulator of Abl, we demonstrate here for the first time that Rb is also a substrate of the Abl protein tyrosine kinase and may thus constitute a downstream effector of Abl. Abl and its downstream effectors are necessary for survival of CML cells, and a specific inhibitor of Abl has been used as an anticancer drug that induces apoptosis in CML cells (Druker *et al*., 2001; Calabretta and Perrotti, 2004; Harata *et al*., 2004). A number of cytoplasmic signal transduction pathways that are normally controlled by receptor tyrosine kinases are activated by Abl; however, most of the studies have been performed by forced expression of Bcr/Abl in established cell lines or mouse models, and may not entirely apply to human tumor cells (Druker *et al*., 2001; Calabretta and Perrotti, 2004). We demonstrate here that endogenous Rb is constitutively phosphorylated at

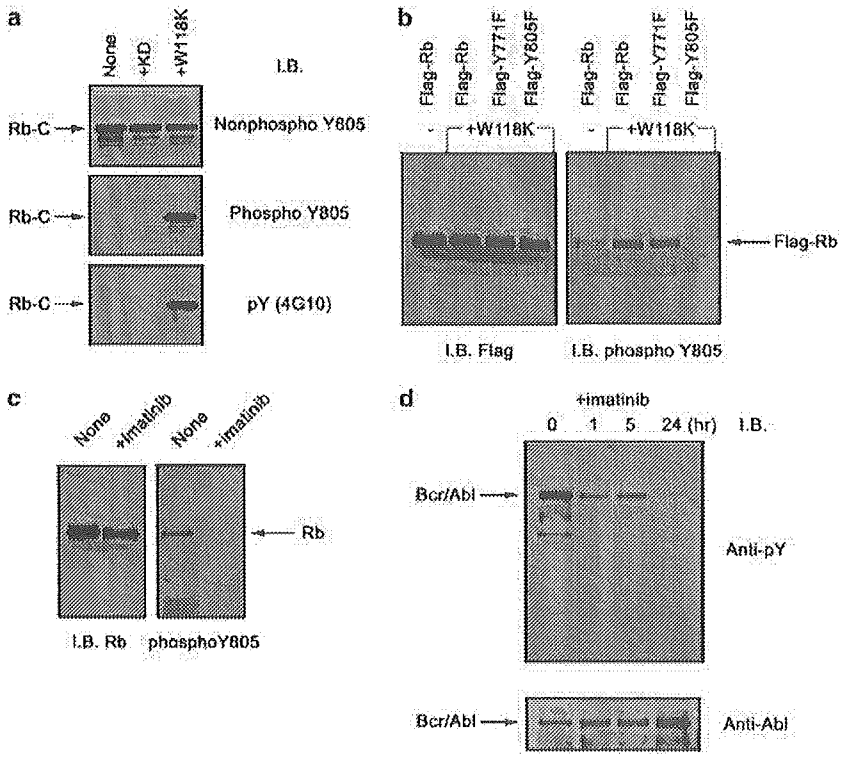

Figure 5 Endogenous Rb is phosphorylated at Y805 in K562 cells. (**a**) GST-Rb-C was incubated with Abl W118K or with KD mutant, followed by immunoblotting with anti-nonphosphoY805 (upper panel), anti-phosphoY805 (middle panel), or with anti-phosphotyrosine (lower panel). (**b**) Flag-tagged Rb and its mutants were coexpressed with W118K in 293-T cells followed by immunoprecipitation with anti-Flag and immunoblotting with anti-Flag (left panel) or anti-phosphoY805 (right panel). (**c**) Endogenous Rb protein was immunoprecipitated from K562 cells grown in the presence or absence of imatinib (1 μM) for 24 h followed by immunoblotting with anti-Rb (left panel) and with anti-phosphoY805 (right panel). (**d**) Endogenous Bcr/Abl protein was immunoprecipitated from K562 cells grown in the presence of imatinib (1 μM) for the indicated time, followed by immunoblotting with anti-phosphotyrosine (upper panel) or with anti-Abl (lower panel).

tyrosine in Bcr/Abl-positive human tumor cell lines and serves as a survival factor in those cells. This raises the possibility that tyrosine-phosphorylated Rb could be a molecular target for cell-type-specific cancer therapy aimed at inducing apoptosis in Abl-dependent tumor cells.

Our findings suggest that excess Rb induces apoptosis in Abl-dependent tumor cells by inhibiting the tyrosine kinase activity of Abl, and that Abl-catalysed phosphorylation of Rb at Y805 is necessary for survival of Abl-dependent tumor cells. Our results also imply that, besides Rb, there are additional downstream targets of Abl tyrosine kinase required for survival of Abl-dependent tumor cells, because the replacement of Tyr-805 by Phe in Rb did not suppress the W118K-induced apoptosis completely and, likewise, the replacement of Tyr-805 by Asp reduced apoptosis only to a partial extent (Figure 7). Since it has been reported that Rb binds to the catalytic domain of Abl (Wang, 2000), it is likely that excess Rb competes with additional downstream targets of Abl required for survival of Abl-dependent tumor cells.

Previous reports showed that expression of Rb in Rb-negative prostate cancer cells sensitized the cells to apoptosis (Bowen *et al*., 2002), and that phosphorylation of Rb at S567 triggered apoptosis in tumor cells (Ma *et al*., 2003). However, these results are somewhat contradictory to the observation that Rb−/− mice die with widespread apoptosis during embryogenesis, and restoration of the caspase-resistant mutant of Rb in Rb−/− cells or mice protects against apoptosis in a signal- and tissue-dependent manner (Harbour and Dean, 2000; Chau *et al*., 2002). We do not yet have an explanation for the apparently different roles of Rb in apoptosis; however, they may result from multiple forms of Rb that arise via post-translational modification, such as site-specific phosphorylation, which may vary in different tumor cell types.

We note that the site of Abl-catalysed phosphorylation, Y805, is located in the C-terminal domain of Rb, which regulates protein–protein interactions. Rb function is regulated by site-specific phosphorylation at serine/threonine in the C-terminal domain (Knudsen and Wang, 1997; Harbour *et al*., 1999), and phosphorylation of the C-terminal domain by cyclin-dependent kinase 4/6 initiates intramolecular interactions between the C-terminal domain and the B domain of Rb, resulting in dissociation of E2F (Knudsen and Wang,

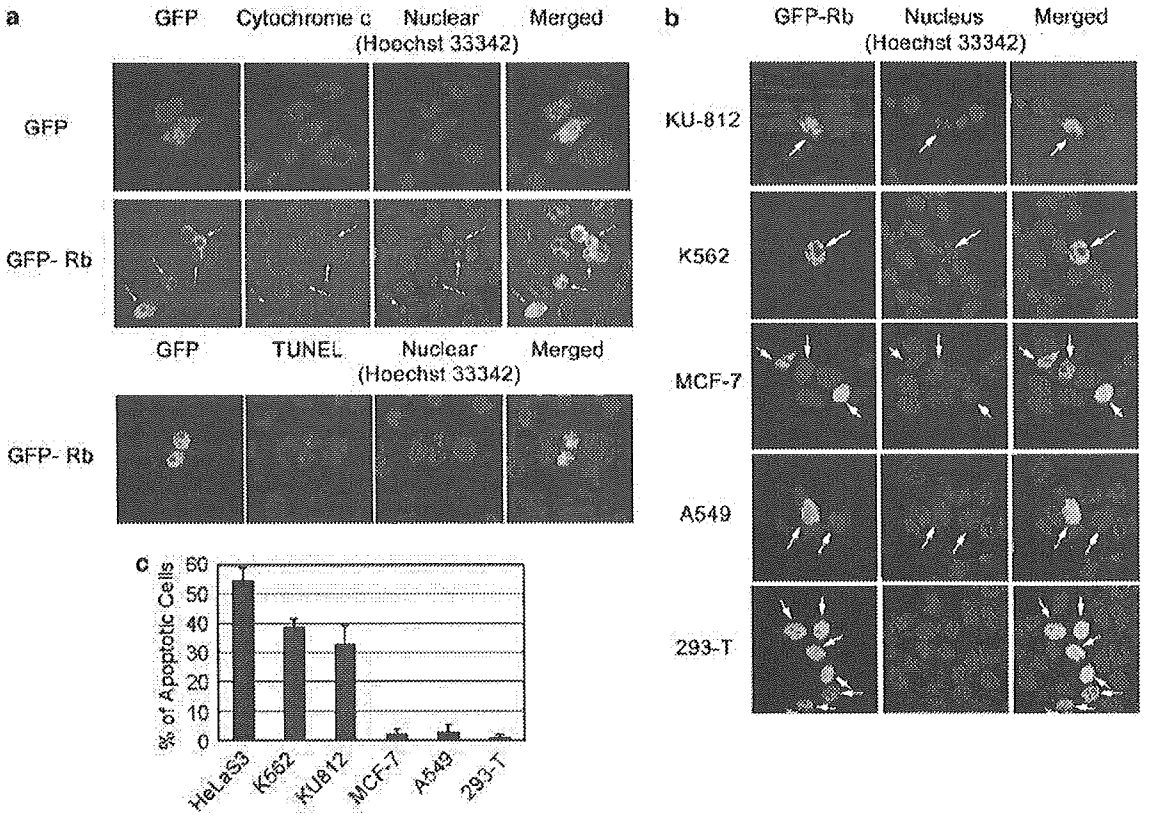

Figure 6 Induction of apoptosis by ectopic expression of Rb. (**a**) GFP or GFP-tagged Rb was overexpressed in HeLa S3 cells. A day after transfection, cells were stained with Hoechst 33342 and anti-cytochrome *c* (upper and middle panels) or subjected to TUNEL assay (lower panel). Arrows indicate typical apoptotic cells exhibiting condensed nuclei (strong staining with Hoechst 33342), release of cytochrome *c* from mitochondria to cytoplasm, and DNA fragmentation (TUNEL staining). (**b**) GFP-tagged Rb was overexpressed in KU-812, K562, MCF-7, A549, and 293-T cells. At 1 or 2 days after transfection, cells were stained with Hoechst 33342. (**c**) The percentage of apoptotic cells was quantitated as described under Materials and methods. Values are the mean±s.e.m. of triplicate experiments. Similar result was obtained in another independent experiment.

1997; Harbour *et al*., 1999). Recent studies also show that Rb function is regulated by acetylation at lysine in the C-terminal domain during differentiation of monocytes and muscle cells (Chan *et al*., 2001; Nguyen *et al*., 2004). We propose that tyrosine phosphorylation of the C-terminal domain is an additional mechanism by which Rb function is regulated, thereby potentially altering the interaction of Rb with other proteins, leading to tumorigenesis. Since Rb binds numerous proteins and forms large protein complexes (Weinberg, 1995; Sherr, 1996; Harbour and Dean, 2000), it is possible that tyrosine phosphorylation induces a conformational change in Rb that modifies the protein–protein interactions, thereby enabling Rb to express its function in survival of tumor cells. Although a direct link between tyrosine-phosphorylated Rb and the survival pathway in tumor cells remains to be elucidated, our results imply that post-translational modification of Rb may serve as a mechanism to determine cell fate (i.e., serine/threonine phosphorylation for growth, lysine acetylation for differentiation, and tyrosine phosphorylation for inhibition of apoptosis). Dysregulation of Rb may thus result in an undesirable cell fate decision that leads to tumorigenesis. More detailed proteomic analyses of the spatiotemporal regulation of protein interactions involving Rb and its dynamic changes by post-translational modifications will clarify our understanding of the regulation of cell fate and the mechanisms of tumorigenesis.

Materials and methods

Cell culture

HeLa S3 cells were obtained from the American Type Culture Collection (Manassas, VA, USA). MCF-7 (JCRB0134), A549 (JCRB0076), KU812 (JCRB0104), and K562 (JCRB0019) cells were obtained from the Japan Health Sciences Foundation (Osaka, Japan). HeLa S3 cells were maintained in Joklik's modified minimum essential medium (MEM) (JRH Biosciences, Lenexa, KS, USA) supplemented with 10% FCS. 293-T cells were grown in DMEM (Invitrogen, Carlsbad, CA, USA) supplemented with 10% FCS. KU812 and K562 cells were maintained in RPMI1640 (Sigma-Aldrich, Inc., St Louis, MO, USA) supplemented with 10% FCS. A549 was maintained in MEM α (Invitrogen) supplemented with 10%

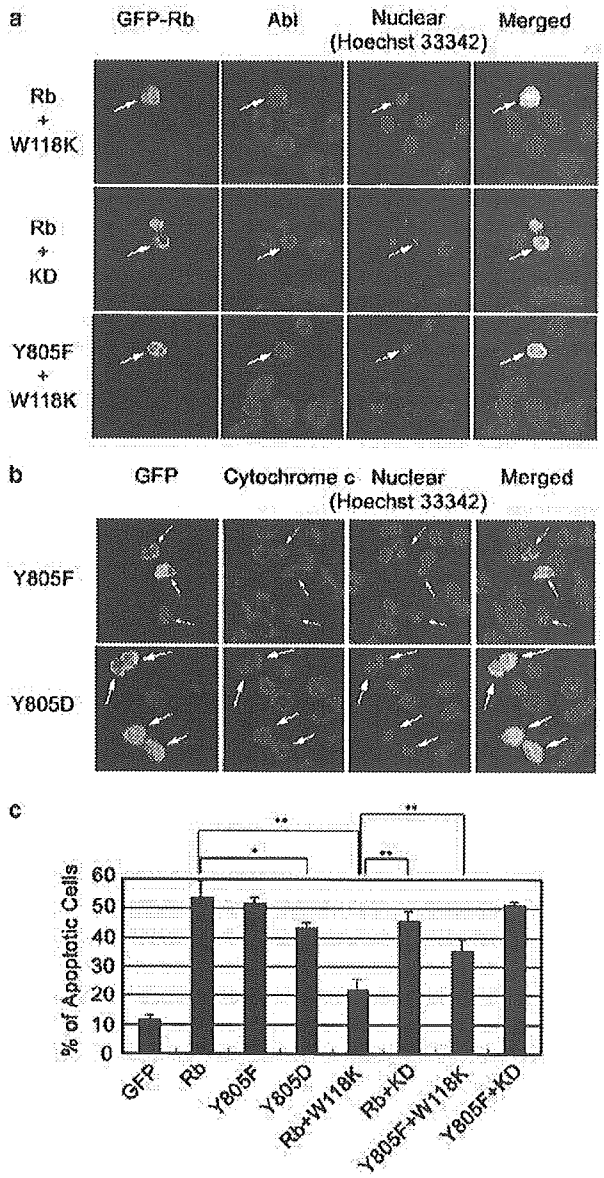

Figure 7 Rb-induced apoptosis is compromised by phosphorylation of Y805 by Abl. (**a**) GFP-Rb or Y805F, which mimics a nonphosphorylated form of Rb, was coexpressed with W118K or KD and stained with anti-Abl and Hoechst 33342 to examine the induction of apoptosis in cotransfected cells. (**b**) Y805 F or Y805D, which mimics a phosphorylated form of Rb, was overexpressed and stained with Hoechst 33342 and anti-cytochrome *c*. (**c**) The percentage of apoptotic cells was determined as described in Materials and methods. Values are the mean ± s.e.m. of triplicate experiments. Similar results were obtained in at least three independent experiments. $^{*}P<0.05$; $^{**}P<0.01$ (Student's *t*-test).

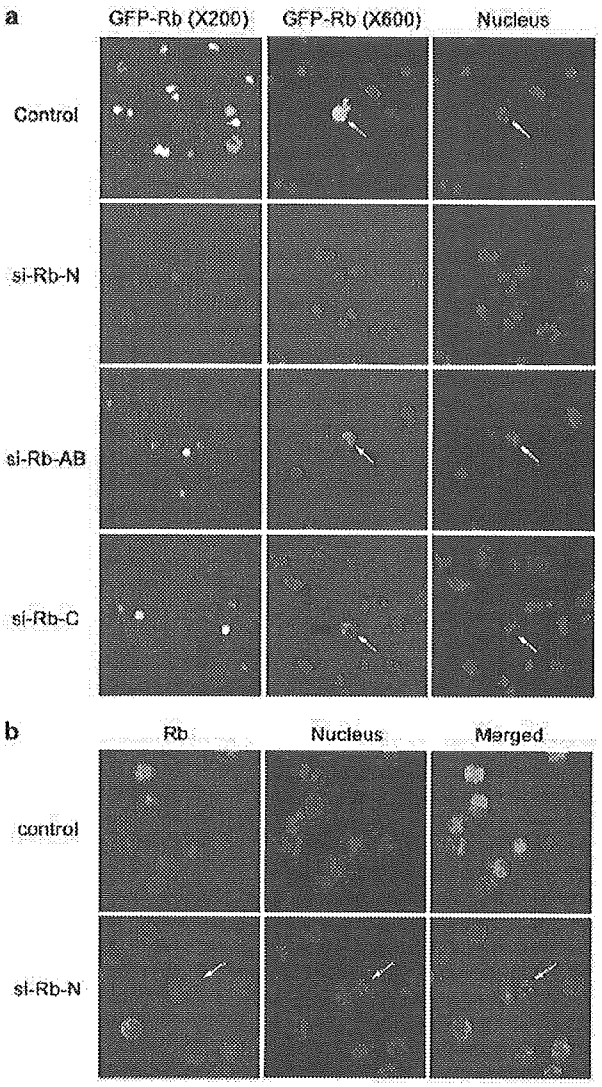

Figure 8 Silencing of endogenous Rb-induced apoptosis in K562 cells. (**a**) Control lacZ si-RNA and three distinct RNAi constructs (si-Rb-N, si-Rb-AB, and si-Rb-C; Materials and methods) were transfected with GFP-Rb, and the cells were stained with 2 μg/ml Hoechst 33342 (left panel; × 200 magnification, right panel; × 600 magnification). (**b**) Control lacZ si-RNA and si-Rb-N were transfected, and the cells were stained with anti-Rb and Hoechst 33342 to examine the induction of apoptosis in the Rb-silenced cells.

FCS. MCF-7 was maintained in MEM α supplemented with 10% FCS and 10 μg/ml insulin.

Plasmids

Full-length Rb was generated from total RNA of HeLa S3 cells by RT–PCR and subcloned into pGEX4T-1 (Amersham Biosciences, Piscataway, NJ, USA), pGFP-C1 (BD Biosciences, San Jose, CA, USA), or a Flag-tagged vector, pCMV-Tag 3 (Stratagene, La Jolla, CA, USA). The entire coding region of Rb was proved to have no mutations in the nucleotide sequence. Site-directed mutagenesis was performed with Gene Tailor Site-Directed Mutagenesis System (Invitrogen) according to the manufacturer's protocol. Abl constructs were kindly provided by Drs T Shishido (Nara Institute of Science and Technology, Nara, Japan) and D Baltimore (Shishido *et al*., 2000) (California Institute of Technology, Pasadena, CA, USA).

Immunoprecipitation and immunoblotting

For immunoprecipitation, cells were lysed in a buffer containing 50 mM Tris-HCl (pH 7.4), 150 mM NaCl, 1% NP-40,

protease inhibitor cocktail (Roche, Basel, Switzerland), 1 mM sodium orthovanadate, and the lysate was incubated with anti-mouse IgG, anti-Rb (IF8) conjugated to agarose (Santa Cruz Biotechnology Inc., Santa Cruz, CA, USA), anti-phosphotyrosine (PY20) (BD Biosciences), and anti-Flag M2 (Sigma-Aldrich Inc.) mouse monoclonal antibodies for 1 h or overnight, followed by incubation with protein A- or G-agarose (Pierce, Rockford, IL, USA) for 1 h at 4°C. After extensive washes with lysis buffer, immunoprecipitates were eluted with 0.2 M glycine (pH 2.5) or SDS sample buffer (62.5 mM Tris-HCl, pH 6.8, 20% glycerol, 2% SDS, 5% β-mercaptoethanol) and resolved by SDS–PAGE, followed by immunoblotting with anti-Rb (G3-245) (BD Biosciences), anti-phosphotyrosine (4G10) (Upstate Biotechnology, Lake Placid, NY, USA) mouse monoclonal antibodies, or anti-Abl rabbit polyclonal antibody (K-12) (Santa Cruz Biotechnology Inc.). Proteins were visualized with ECL Western Blotting Detection reagents (Amersham Biosciences).

In-gel digestion and MS analysis

In-gel tryptic digests of protein bands were performed with the Montage In-Gel Digest kit (Millipore, Bedford, MA, USA) according to the manufacturer's protocol. The peptide mixture was then analysed by tandem MS on an electrospray ionization quadruple time-of-flight mass spectrometer (Q-TOF2, Micromass, Manchester, UK) equipped with nano-flow liquid chromatography as described previously (Taoka *et al*., 2003). All spectra were analysed with Mascot software (Matrix Science, London, UK) to search the nonredundant protein database compiled by the National Center for Biotechnology Information.

In vitro *kinase assay*

The *in vitro* kinase assay was performed as described previously (Lewis *et al*., 1996). Briefly, 293-T cells were grown on a 10-cm dish and transfected with Abl constructs. A day after transfection, cells were harvested and the lysates were immunoprecipitated with anti-Abl (K-12). The immunoprecipitates were washed and resuspended in kinase buffer (10 mM Tris-HCl, pH 7.4, 10 mM $MgCl_2$, 1 mM DTT) containing GST-Rb-C. Kinase reactions were initiated by adding 10 μM unlabeled ATP and 1 μCi of [γ-^{32}P]ATP. After incubating 30 min at room temperature, reactions were stopped by adding SDS sample buffer. Proteins were then separated by SDS–PAGE, followed by Coomassie brilliant blue (CBB) staining with SimplyBlue Safe Stain (Invitrogen) or direct autoradiography.

Transfection, immunofluorescence staining, and assessment of apoptotic cells

Cells were transfected transiently with Lipofectamine Plus, DMRIE-C reagents, or a Calcium Phosphate Transfection kit (Invitrogen) according to the manufacturer's protocols. For immunofluorescence staining, cells were grown on coverslips in six-well plates and fixed by adding formaldehyde (3.7% final concentration) to the medium. Fixed cells were then permeabilized with PBS containing 0.2% Triton X-100, followed by incubation in blocking solution (PBS with 1% BSA and 1% FCS) for 30 min at room temperature. Cells were washed and then incubated with anti-cytochrome *c* (6H2.B4) (BD Biosciences), anti-Rb (G3-245) mouse monoclonal antibodies, or anti-Abl rabbit polyclonal antibody (K-12) for 1 h, followed by incubation with secondary antibodies conjugated to fluorescein or rhodamine and visualized with a Radiance 2100 confocal microscope (Bio-Rad, Hercules, CA, USA). Apoptotic cells were assessed by staining with 2 μg/ml Hoechst 33342 (Molecular Probes, Eugene, OR, USA), and the proportions of apoptotic nuclei were determined by scoring at least 100 GFP-positive cells with nuclei stained with Hoechst 33342 for apoptotic features. The TUNEL assay was performed using the *In Situ* Cell Death Detection kit (Roche) according to the manufacturer's protocol.

Generation of phospho-Rb (Y805)-specific antibody

The antibody was raised in rabbits against a synthetic phosphopeptide antigen PGGNIY*ISPLKC, where Y* represents phosphotyrosine (Sigma Genosys, Hokkaido, Japan). The phosphopeptide-reactive antiserum was first purified by affinity chromatography on a phosphopeptide-bound Sepharose, and further purified by passing the antibody through a Sepharose column bound with the nonphosphopeptide.

RNA interference

Silencing of Rb was performed with BLOCK-iT Dicer RNAi kit (Invitrogen) according to the manufacturer's protocol. The nucleotide fragments encoding N-terminal (nucleotides 456–1275: 820 bp), A/B (nucleotides 1252–1809: 558 bp), and C-terminal domains (nucleotides 2201–2938: 738 bp) of Rb were amplified by PCR, and the linear sense and antisense DNA templates of PCR products were subjected to *in vitro* transcription to generate single-stranded RNA (ssRNA). ssRNA was then annealed to generate double-stranded RNA (dsRNA), followed by dicing reaction. Diced siRNAs generated from N-terminal, A/B, and C-terminal domain of Rb (designated as si-Rb-N, si-Rb-AB, and si-Rb-C, respectively) and a diced control lacZ si-RNA were transfected with Lipofectamine 2000 (Invitrogen) into K562 cells according to the manufacturer's protocol. At 2 days after transfection, the cells were stained with anti-Rb and Hoechst 33342.

Acknowledgements

We thank Drs T Shishido and D Baltimore for providing Abl constructs, Novartis Pharmaceuticals Corporation for imatinib, and Ms N Okamura and S Hamada for the technical assistance. The Division of Proteomics Research is supported by Applied Biosystems, Japan and Millipore Corporation.

References

Baltimore D, Ren R, Cheng G, Alexandropoulos K, Cicchetti P. (1995). *Ann NY Acad Sci* **758**: 339–344.

Baskaran R, Wood LD, Whitaker LL, Canman CE, Morgan SE, Xu Y *et al*. (1997). *Nature* **387**: 516–519.

Bowen C, Birrer M, Gelmann EP. (2002). *J Biol Chem* **277**: 44969–44979.

Brehm A, Miska EA, McCance DJ, Reid JL, Bannister AJ, Kouzarides T. (1998). *Nature* **391**: 597–601.

Calabretta B, Perrotti D. (2004). *Blood* **103**: 4010–4022.

Chan HM, Krstic-Demonacos M, Smith L, Demonacos C, La Thangue NB. (2001). *Nat Cell Biol* **3**: 667–674.

Chau BN, Borges HL, Chen TT, Masselli A, Hunton IC, Wang JY. (2002). *Nat Cell Biol* **4**: 757–765.

Cujec TP, Medeiros PF, Hammond P, Rise C, Kreider BL. (2002). *Chem Biol* **9**: 253–264.

Druker BJ, Talpaz M, Resta DJ, Peng B, Buchdunger E, Ford JM *et al*. (2001). *N Engl J Med* **344**: 1031–1037.

Guo XY, Balague C, Wang T, Randhawa G, Yuan Z, Bachier C *et al.* (1999). *Oncogene* **18**: 1589–1595.
Harata M, Soda Y, Tani K, Ooi J, Takizawa T, Chen M *et al.* (2004). *Blood* **104**: 1442–1449.
Harbour JW, Dean DC. (2000). *Nat Cell Biol* **2**: E65–E67.
Harbour JW, Luo RX, Dei Santi A, Postigo AA, Dean DC. (1999). *Cell* **98**: 859–869.
Helin K, Harlow E, Fattaey A. (1993). *Mol Cell Biol* **13**: 6501–6508.
Horowitz JM, Yandell DW, Park SH, Canning S, Whyte P, Buchkovich K *et al.* (1989). *Science* **243**: 937–940.
Janicke RU, Walker PA, Lin XY, Porter AG. (1996). *EMBO J* **15**: 6969–6978.
Knudsen ES, Wang JY. (1997). *Mol Cell Biol* **17**: 5771–5783.
Lewis JM, Baskaran R, Taagepera S, Schwartz MA, Wang JY. (1996). *Proc Natl Acad Sci USA* **93**: 15174–15179.
Luo RX, Postigo AA, Dean DC. (1998). *Cell* **92**: 463–473.
Ma D, Zhou P, Harbour JW. (2003). *J Biol Chem* **278**: 19358–19366.
Magnaghi-Jaulin L, Groisman R, Naguibneva I, Robin P, Lorain S, Le Villain JP *et al.* (1998). *Nature* **391**: 601–605.
Nevins JR. (1992). *Science* **258**: 424–429.
Nguyen DX, Baglia LA, Huang SM, Baker CM, McCance DJ. (2004). *EMBO J* **23**: 1609–1618.
Onadim Z, Hogg A, Baird PN, Cowell JK. (1992). *Proc Natl Acad Sci USA* **89**: 6177–6181.
Sellers WR, Rodgers JW, Kaelin Jr WG. (1995). *Proc Natl Acad Sci USA* **92**: 11544–11548.
Shafman T, Khanna KK, Kedar P, Spring K, Kozlov S, Yen T *et al.* (1997). *Nature* **387**: 520–523.
Sherr CJ. (1996). *Science* **274**: 1672–1677.
Shishido T, Akagi T, Ouchi T, Georgescu MM, Langdon WY, Hanafusa H. (2000). *Proc Natl Acad Sci USA* **97**: 6439–6444.
Taagepera S, McDonald D, Loeb JE, Whitaker LL, McElroy AK, Wang JY *et al.* (1998). *Proc Natl Acad Sci USA* **95**: 7457–7462.
Tan X, Wang JY. (1998). *Trends Cell Biol* **8**: 116–120.
Taoka M, Ichimura T, Wakamiya-Tsuruta A, Kubota Y, Araki T, Obinata T *et al.* (2003). *J Biol Chem* **278**: 5864–5870.
Wang JY. (2000). *Oncogene* **19**: 5643 5650.
Weinberg RA. (1995). *Cell* **81**: 323–330.
Wen ST, Jackson PK, Van Etten RA. (1996). *EMBO J* **15**: 1583–1595.
Zhang J, Gray J, Wu L, Leone G, Rowan S, Cepko CL *et al.* (2004). *Nat Genet* **36**: 351–360.

Supplementary Information accompanies the paper on the Oncogene website (http://www.nature.com/onc).

STEM CELLS®
Original Article

Establishment of Novel Embryonic Stem Cell Lines Derived from the Common Marmoset (*Callithrix jacchus*)

ERIKA SASAKI,[a] KISABURO HANAZAWA,[b] RYO KURITA,[c] AKIRA AKATSUKA,[d] TAKAHITO YOSHIZAKI,[e] HAJIME ISHII,[a] YOSHIKUNI TANIOKA,[a] YASUYUKI OHNISHI,[f] HIROSHI SUEMIZU,[f] AYAKO SUGAWARA,[g] NORIKAZU TAMAOKI,[f] KIYOKO IZAWA,[h] YUKOH NAKAZAKI,[c] HIROMI HAMADA,[i] HIROFUMI SUEMORI,[j] SHIGETAKA ASANO,[h] NORIO NAKATSUJI,[k] HIDEYUKI OKANO,[e] KENZABURO TANI[c]

[a]Division of Laboratory Animal Science, Central Institute for Experimental Animals, Kawasaki, Kanagawa, Japan; [b]Department of Urology, Urayasu Hospital, Juntendo University, Urayasu, Chiba, Japan; [c]Department of Molecular Genetics, Division of Molecular and Clinical Genetics, Medical Institute of Bioregulation, Kyushu University, Hakata, Fukuoka, Japan; [d]Tokai University School of Medicine, Isehara, Kanagawa, Japan; [e]Department of Physiology, Keio University School of Medicine, Shinjuku-ku, Tokyo, Japan; [f]Research Project Center, [g]Department of Genetics, Central Institute for Experimental Animals, Kawasaki, Kanagawa, Japan; [h]Division of Molecular Therapy, Institute of Medical Science, University of Tokyo, [i]Institute of Obstetrics & Gynecology in Clinical Medicine, University of Tsukuba, [j]Laboratory of Embryonic Stem Cell Research, Stem Cell Research Center, [k]Department of Development and Differentiation, Institute for Frontier Medical Sciences, Kyoto University, Kyoto, Japan

Key Words. Embryonic stem cells • Common marmoset • Embryoid body • Nonhuman primate • Teratoma formation

ABSTRACT

The successful establishment of human embryonic stem cell (hESC) lines has inaugurated a new era in regenerative medicine by facilitating the transplantation of differentiated ESCs to specific organs. However, problems with the safety and efficacy of hESC therapy in vivo remain to be resolved. Preclinical studies using animal model systems, including nonhuman primates, are essential to evaluate the safety and efficacy of hESC therapies. Previously, we demonstrated that common marmosets are suitable laboratory animal models for preclinical studies of hematopoietic stem cell therapies. As this animal model is also applicable to preclinical trials of ESC therapies, we have established novel common marmoset ESC (CMESC) lines. To obtain marmoset embryos, we developed a new embryo collection system, in which blastocysts can be obtained every 3 weeks from each marmoset pair. The inner cell mass was isolated by immunosurgery and plated on a mouse embryonic feeder layer. Some of the CMESC lines were cultured continuously for more than 1 year. These CMESC lines showed alkaline phosphatase activity and expressed stage-specific embryonic antigen (SSEA)-3, SSEA-4, TRA-1-60, and TRA-1-81. On the other hand, SSEA-1 was not detected. Furthermore, our novel CMESCs are pluripotent, as evidenced by in vivo teratoma formation in immunodeficient mice and in vitro differentiation experiments. Our established CMESC lines and the common marmoset provide an excellent experimental model system for understanding differentiation mechanisms, as well as the development of regenerative therapies using hESCs. STEM CELLS *2005;23:1304–1313*

Correspondence: Kenzaburo Tani, M.D., Ph.D., Department of Molecular Genetics, Division of Molecular and Clinical Genetics, Medical Institute of Bioregulation, Kyushu University, Hakata, Fukuoka 812-8582, Japan. Telephone: 81-92-642-6434; Fax: 81-92-642-6444; e-mail: taniken@bioreg.kyushu-u.ac.jp; for CMES cell distribution, contact Erika Sasaki at esasaki@ciea.or.jp Received December 22, 2004; accepted for publication May 5, 2005; first published online in STEM CELLS *EXPRESS* August 18, 2005. 1066-5099/2005/$12.00/0 doi: 10.1634/stemcells.2004-0366

Introduction

Embryonic stem cells (ESCs) are derived from preimplantation embryos. Owing to their pluripotency, ESCs have been widely used for the production of transgenic and gene knockout mice to elucidate the molecular mechanisms of various genes. In 1998, the successful establishment of human ESC (hESC) lines enhanced the role of ESCs in science and medicine. The most promising application of ESCs in the clinical setting is in the repair of defective organ function by differentiated ESCs. However, before differentiated hESCs can be used in clinical applications, the short-term and long-term safety and efficacy of ESCs must be thoroughly examined. Due to ethical considerations, these studies cannot be performed in vivo in humans. Therefore, preclinical studies using the ESCs of nonhuman primates are essential.

The common marmoset (*Callithrix jacchus*) is a New World primate species with reproductive characteristics that are appropriate for ESC studies. More specifically, these animals are small (weighing approximately 350–400 g), they have a short gestation period (approximately 144 days), and reach sexual maturity at 12–18 months. Unlike macaques, marmosets routinely deliver twins or triplets for each pregnancy. In addition, it is possible to synchronize the marmoset ovarian cycle with prostaglandin analogs, collect age-matched embryos from multiple females, and transfer embryos to synchronized recipients with success rates in the range of 70%–80% [1–3]. Because these reproductive characteristics allow routine efficient transfer of multiple embryos, marmosets constitute an excellent primate species for the generation of transgenic and knockout animal models of human diseases.

In addition to these reproductive benefits, we have shown previously that marmosets are suitable laboratory animals for preclinical studies of stem cell therapies, owing to the similarities between the hematopoietic and immune systems of humans and marmosets [4, 5]. In 1996, Thomson et al. [6] established pluripotent common marmoset cell lines, which are considered powerful tools for understanding the regulatory mechanisms of ESC differentiation both in vitro and in vivo. However, the differentiation abilities of the pluripotent common marmoset cells in terms of in vitro teratoma formation assays and certain common properties of ESC lines, such as differentiation to the cell lineages of three germ layers, have not been defined fully. The establishment of totipotent common marmoset ESC (CMESC) lines would facilitate the construction, by gene targeting, of nonhuman primate models for human disease. To achieve our goal of establishing the common marmoset as a human disease model, we have established novel CMESC lines and characterized their differentiation capacities.

Materials and Methods

Animals

To obtain marmoset embryos, 15 pairs of common marmosets, older than 2 years of age, were selected from the marmoset breeding colony; this colony has been maintained in our laboratory at the Central Institute for Experimental Animals (CIEA) since 1975. Each pair was kept in a cage with dimensions of 39 × 60 × 70 cm. This study was approved by the animal ethics committees of CIEA and was performed in accordance with CIEA guidelines.

Embryo Collection

Fifteen female animals were divided into three groups. The ovulation cycles of each group of animals were synchronized with the prostaglandin (PG) F2α analogue cloprostenol (0.75 mg/head Estrumate; Schering-Plough Animal Health, Union, NJ, http://www.spah.com) which was administered more than 10 days after the luteal phase, as reported previously [7]. Plasma samples (0.1 ml) were collected from the femoral vein at 2, 9, 11, and 13 days after the injection of cloprostenol, and the day of ovulation was determined by the plasma progesterone concentration, using an enzyme immunoassay (EIA), as described below. The day of ovulation (day 0) was defined as the day before the serum progesterone level reached 10 ng/ml [8]. Embryos were collected 7–10 days after ovulation, after anesthesia by intramuscular injection of 0.05 mg per head of medetomidine hydrochloride (Domitor; Meiji Techno, Tokyo, http://www.meijitechno.co.jp) or 0.25–0.5 mg per head of flunitrazepam (Silece; Eisai Co., Ltd., Tokyo, http://www.eisai.co.jp/index-e.html) and 70 mg per head of ketamine hydrochloride (veterinary Ketalar 50; Sankyo Lifetech Co., Ltd., Tokyo, http://www.sankyo-lifetech.co.jp/english). The cervix and both oviducts were exteriorized by midline laparotomy and clamped, and the uterine lumen was flushed from the proximal end to the cervix with 2.5 ml of Dulbecco's modified Eagle's medium (DMEM; Invitrogen, Tokyo, http://www.invitrogen.com) that contained 10% fetal bovine serum (FBS; JRH, Tokyo, http://www.jrhbio.com). The flushed medium was collected using a 23-gauge needle that was placed in the uterine lumen through the uterine fundus. Cloprostenol was also administered 4 days after embryo collection. The plasma progesterone concentration was determined using the DPC Progesterone Kit (Diagnostic Products Corporation, Los Angeles, http://www.dpcweb.com) according to the recommendations of the manufacturer.

Isolation and Culture of ESC Lines

Inner cell masses (ICMs) were isolated by immunosurgery, as described previously [9]. Briefly, the zona pellucida of the marmoset blastocyst was removed by the addition of 0.5% pronase (Sigma, Tokyo, http://www.sigmaaldrich.com) in DMEM, and the blastocysts were washed three times with DMEM. To remove the trophectoderm, the blastocysts were incubated for 45 minutes at 37°C in 5% CO_2 with a 10-fold dilution of anti-marmoset fibroblast rabbit serum in DMEM. After three washes with DMEM, the blastocysts were incubated with a fivefold dilution of guinea pig complement (Invitrogen) in DMEM for 30 minutes at 37°C in 5% CO_2. After immunosurgery, the trophectoderm was removed by pipet-

ting, and the ICMs were isolated. The ICMs were plated on 3,500-rad γ-irradiated mouse embryonic fibroblast (MEF) feeder layer. After 10–14 days, the ICMs were dissociated in trypsin-EDTA and replated on a fresh MEF feeder layer. The ICMs and their expanded cells were cultured using CMESC medium that consisted of 80% Knockout DMEM supplemented with 20% Knockout Serum Replacement (KSR; Invitrogen), 1 mM L-glutamine, 0.1 mM MEM nonessential amino acids, 0.1 mM β-mercaptoethanol (2-ME; Sigma), 100 IU/ml penicillin, 100 μg/ml streptomycin sulfate, 250 ng/ml amphotericin B, and 10 ng/ml leukemia inhibitory factor. For cell splitting, undifferentiated CMESC colonies were detached from the feeder cells, using 0.25% trypsin that was supplemented with 1 mM $CaCl_2$ and 20% KSR. The removed colonies were mechanically dissociated into 10 to 50 cells and replated on new irradiated MEF feeder layer.

Immunohistochemical Staining

To examine the expression of cell surface markers on cultured marmoset ICMs, alkaline phosphatase was detected using the Alkaline Phosphatase Staining Kit (Sigma) according to the manufacturer's instructions. For immunostaining, ESCs were fixed with 4% paraformaldehyde in phosphate-buffered saline (PBS) for 10 minutes at room temperature and then incubated with 0.3% H_2O_2 for 10 minutes at room temperature. The primary antibodies against stage-specific embryonic antigen (SSEA)-1, SSEA-3, SSEA-4 (Developmental Studies Hybridoma Bank, Iowa City, IA, http://www.uiowa.edu/~dshbwww), TRA-1-60, and TRA-1-81 (Chemicon, Temecula, CA, http://www.chemicon.com) were diluted with Antibody Diluent (DAKO ChemMate; DakoCytomation, Glostrup, Denmark, http://www.dakocytomation.dk) and incubated for 1 hour at room temperature. The following primary antibodies (dilutions) were used: anti-SSEA-1 (1:50), anti-SSEA-3 (1:10), anti-SSEA-4 (1:50), anti-TRA-1-60, and anti-TRA-1-81 (10 μg/ml). After three washes with PBS, the biotinylated secondary antibody Simple Stain PO Multi system (Nichirei Corporation, Tokyo, http://www.nichirei.co.jp/english) was incubated with the cells for 30 minutes at room temperature. The samples were washed three times with PBS, and the localization of the bound monoclonal antibodies was detected using the DAB (3,3'-diaminobenzidine tetrahydrochloride) horseradish peroxidase complex.

For immunohistochemical analysis of tumors that formed after transplantation into immunodeficient mice, the collected tumors were fixed in neutral buffered formalin and embedded in paraffin. The paraffin blocks were sectioned and subjected to immunohistochemical staining. Primary antibodies against keratin wide specific screening (WSS), desmin, CD31, and glial fibrillary acidic protein (GFAP) (all purchased from DakoCytomation, Tokyo) were incubated with the paraffin sections at dilutions of 1:200, 1:200, 1:10, and 1:50, respectively. The localization of the bound monoclonal antibodies was detected using the Envision System (DakoCytomation).

For immunofluorescence staining of in vitro–differentiated neural cells, the slides and sections were preincubated with 10% normal goat serum plus 0.3% Triton X-100 in PBS, followed by overnight incubation in 10% normal goat serum plus 0.3% Triton X-100 in PBS that contained rabbit polyclonal anti-TH antibody (AB152; Chemicon). Alexa™ 488 goat anti-rabbit IgG antibody and Alexa™ 568 goat anti-mouse IgG antibody (Jackson ImmunoResearch Laboratories, Inc., West Grove, PA, http://www.jacksonimmuno.com) were added as secondary antibodies for 2 hours. Finally, the specimens were soaked in 2 μg/ml Hoechst 33528 in distilled water. All of the micrographs were analyzed on the Zeiss AxioCam imaging system (Carl Zeiss, Jena, Germany, http://www.zeiss.com).

Karyotypic Analysis

ESCs were prepared by passaging a confluent culture from a 25-cm^2 bottle. After a 3-hour incubation with fresh medium, a colcemid (Invitrogen) was added to a final concentration of 0.02 μg/ml for 20 minutes. The cells were then washed in PBS, dissociated using trypsin, and spun down. The pellet was resuspended carefully in 0.56% KCl at room temperature. After centrifugation, the hypotonic solution was removed, and the pellet was fixed with methanol/acetic acid, 3:1 (vol/vol) via gently pipetting. After centrifuging at 1,000 rpm, 5-minute fixation was performed twice before spreading the cells on slides. The slides were air-dried overnight, stained in freshly made 5% Giemsa for 10 minutes, and rinsed with distilled water. In the Giemsa (G)-banding analysis, the numbers of chromosomes as well as karyotypic analysis were performed using 30 and five metaphase spreads, respectively.

Telomerase Activity

Telomerase activity was determined using the TRAPEZE Telomerase Detection Kit (Chemicon, Tokyo) according to the manufacturer's instructions. Briefly, cell extracts were obtained from approximately 1×10^6 cells, and the protein concentrations were normalized using the Coomassie blue–stained protein assay reagent bovine serum albumin standards (Pierce, Inc., Rockford, IL, http://www.piercenet.com). Heat-inactivated controls were obtained by incubating the samples at 85°C for 10 minutes. Aliquots (1.5 μg) of the cell extracts were used for polymerase chain reaction (PCR), which was performed according to the manufacturer's instructions. The PCR products were electrophoresed on a 12.5% nondenaturing polyacrylamide gel, and telomerase activity was detected by SYBR green staining (Invitrogen).

PCR–Single Strand Conformation Polymorphism (PCR-SSCP)

SSCP analysis of the major histocompatibility complex-DRB genes was performed as described previously [10]. The following PCR primers were used: MA-DR-2r, 5'-CTCTCCGCGGCACTAGGAAC-3'; and MA-DR-4s, 5'-GCACGTTTCTTGGAGTATAGC-3'.

Reverse Transcription (RT)–PCR

Poly(A)$^+$ RNA was isolated using the QuickPrep Micro mRNA Purification Kit (GE Healthcare, Toyko, http://www4.amershambioscience.com) according to the manufacturer's instructions. First-strand cDNA was synthesized from 1 μg of poly(A)$^+$ RNA from the undifferentiated ESCs, or the embryoid bodies (EBs), using the ImProm-II cDNA Synthesis Kit (Promega, Tokyo, http://www.promega.com). As negative controls, 1 μg of the poly(A)$^+$ RNA was allowed to react with the cDNA synthesis reaction mixture in the absence of the ImProm-II RT. After cDNA synthesis, 1/20 of the cDNA synthesis reaction mixture was used as the template for the PCR. For RT-PCR analysis of fresh ICMs, ICMs were obtained from seven blastocysts and used for poly(A)$^+$ RNA isolation. Half of the isolated poly(A)$^+$ RNA was then used for first-strand cDNA synthesis, and the other half was used as a negative control, as described above.

Individual primers were designed for the target genes. The following (forward and reverse) primer pairs were used: *Nanog*, 5'-AAACAGAAGACCAGAACTGTG-3' and 5'-AGTTGTTTTTCTGCCACCTCT-3'; *Oct3/4*, 5'-CCTGGGGGTTCTATTTGGGA-3' and 5'-TTTGAATGCATGGGAGAGCC-3'; *FoxD3*, 5'-CGACGACGGGCTGGAGGAGAA-3' and 5'-ATGAGCGCGATGTACGAGTA-3'; *Sox-2*, 5'-AGAACCCCAAGATGCACAAC-3' and 5'-GGGCAGCGTGTACTTATCCT-3'; CD34, 5'-AGCCTGTCACCTGGAAATGC-3' and 5'-CGTGTTGTCTTGCTGAATGGC-3'; *Nestin*, 5'-GCCCTGACCACTCCAGTTTA-3' and 5'-GGAGTCCTGGATTTCCTTCC-3'; α-*fetoprotein*, 5'-GCTGGATTGTCTGCAGGATGGGGAA-3' and 5'-TCCCCTGAAGAAAATTGGTTAAAAT-3'; marmoset chorionic gonadotropin (*mCG*) β, 5'-CCCTGTGTGTGTCGCCTTT-3' and 5'-CTAATGGAGGGTCTGCTGGC-3'; *Bex1/Rex3*, 5'-ACAGGCAAGGATGAGAGAAG-3' and 5'-CCCACGTAAACAAGTGACAG-3'; HEB, 5'-ACTGAAACAAAGAAAGGATGAAAACC-3' and 5'-CCCTTTCTATCTTCTGTTCAGGGTTC-3'; *gp130*, 5'-AAACAGAACAGCATCCAGTC-3'and5'-AGTTGAGGCATCTTTGGTCC-3'; leukemia inhibitory factor receptor (LIFR), 5'-TTTCTTGGCATTTACCAGG-3' and 5'-GCTATTTTGGAAGGTGGTG-3'; β-*actin*, 5'-TCCTGACCCTSAAGTACCCC-3'and5'-GTGGTGGTGAAGCTGTAGCC-3'. Except for *CD34*, α-*fetoprotein*, and *mCG*, the expected sizes of the PCR products were estimated from human sequences. The expected PCR products were ~190 bp (*nanog*), ~530 bp (*oct3/4*), ~200 bp (*Sox-2*), ~356 bp (*FoxD3*), ~200 bp (*nestin*), 627 bp (*CD34*), 200 bp (α-*fetoprotein*), ~559 bp (*gp130*), ~269 bp (*Bex1/Rex3*), ~165 bp (*HEB*), 286 bp (*mCG*), ~514 bp (*LIFR*), and 418 bp (β-*actin*). The PCR reaction mixture (25 μl) contained ×1 PCR buffer (10 mM Tris-HCl [pH 9.0], 1.5 mM $MgCl_2$, 50 mM KCl), 0.2 mM dNTP, 0.5 μM of each primer, and 2.5 U *Taq* polymerase. The amplification was performed for 35 cycles of denaturation at 95°C for 1 minute, annealing at 60°C for 30 seconds, and elongation at 72°C. Representative RT-PCR products for each gene were verified by DNA sequencing (data not shown).

Analysis of Differentiation Potency

EB Formation

To study EB formation, undifferentiated ESCs were removed from the MEF feeder layer, dissociated using 0.25% trypsin in PBS with 20% KSR and 1 mM $CaCl_2$, and cultured in bacterial Petri dishes for 10–21 days using DMEM supplemented with 10% FBS. The medium was changed every 2 days.

In Vivo Differentiation Analysis: Teratoma Formation

To examine teratoma formation in mice, between 1–5 × 10^6 CMESCs were injected subcutaneously into the abdomen of 5-week-old immunodeficient mice, NOD/shi-scid, IL-2Rγ^{null} (NOG) mice [11]. Four to eight weeks after the injection, tumors were resected from the mice. The resected tumors were fixed in buffered formaldehyde, embedded in paraffin blocks, and subjected to immunohistochemical and histological examinations.

In Vitro Differentiation

Neural Cells

Stromal PA6 cells were plated on 12-mm coverslips and grown to semiconfluence. On day 0, 5 × 10^4 ESCs were cocultured with the PA6 cells on coverslips in Glasgow's modified Eagle's medium (GMEM) supplemented with 10% KSR, 0.1 mM 2-ME, and 10^{-7} M ascorbate. For the first 10 days of coculture, the medium was changed every 2 days. On day 12, the medium was exchanged for GMEM plus N-2 supplement (Invitrogen) that contained 0.1 mM 2-ME and 10^{-7} M ascorbate, and the culture was continued until day 20. The cells were then fixed with 4% paraformaldehyde in PBS.

Hematopoietic Cells

CMESCs were differentiated into hematopoietic cells by EB formation in Iscove's modified Dulbecco's medium (Invitrogen) that contained 15% FBS, 200 μg/ml transferrin, 10 μg/ml insulin, 50 μg/ml ascorbic acid, and 0.45 mM monothioglycerol. The CMESCs (10^4 cells per 9-cm dish) were cultured without cytokines for 14–18 days and then subjected to hematopoietic colony assays. Hematopoietic colonies were examined by growing differentiated ESC-derived cells (10^5 cells) in Methocult GF$^+$ medium (StemCell Technologies, Vancouver, British Columbia, Canada, http://www.stemcell.com) according to the manufacturer's instructions. After 10–14 days, the colony-forming units (CFU) were counted, and cellular morphology was confirmed microscopically using May-Giemsa staining of cytospun samples.

Results

Establishment of CMESC Lines

The marmosets ovulated 10.7 ± 1.3 days ($n = 70$) after PGF2α administration. Our ovarian cycle control system made it possible to obtain fertilized eggs every 3 weeks from the same animals. Sixty immunosurgically isolated ICMs from 70 blastocysts (the ICM isolation rate was 85.7%) were plated on the irradiated MEF feeder layer, and 11 ICMs were cultured for more than 10 passages (18.3% derivation rate). To date, 3/11 ICM-derived cells have been cultured for more than 1 year. All ICM-derived cells showed flat, packed, and tight colony morphology and a high nucleus:cytoplasm ratio (Figs. 1A, 1B). The morphology of these derived cells was very similar to that of reported primate ESCs, including those from humans and from rhesus and cynomolgus monkeys [12–16]. It has been reported that primate ESCs exhibit spontaneous differentiation during culture and that leukemia inhibitory factor does not maintain the ESCs in the undifferentiated state [13, 14]. The common marmoset ICM-derived cell lines also showed low frequency of differentiation. However, most ICM-derived cells maintained undifferentiated morphology of the cells. It is known that the quality of FBS is critical to the maintenance of undifferentiated primate ESCs; different lots of FBS from the same manufacturer can vary in this respect. Therefore, the chemically defined serum-free supplement KSR was used for the establishment and culture of the marmoset ESCs. The CMESC colonies appeared more packed and tight when KSR was used in the culture; they were flatter in appearance when FBS was used in the medium. To maintain stem cells, the dissociation procedure for cynomolgus ESCs was adopted for subculture of the marmoset ICM-derived cells [14]. With this culture system, continuous cultures of CMESCs have been sustained for more than 1 year.

Characterization of Undifferentiated CMESC Lines

To confirm the undifferentiated status of the ICM-derived cells, all three lines (CMESC 20, 30, and 40) were examined for the expression of cell surface markers that are specific for undifferentiated ESCs. As shown in Figures 1C–1G, the ICM-derived cell lines showed alkaline phosphatase activity (Fig. 1C) and expressed SSEA-3 (Fig. 1E), SSEA-4 (Fig. 1F), TRA-1-60 (Fig. 1G), and TRA-1-81 (Fig. 1H) but not SSEA-1 (Fig. 1D). All three cell lines retained the normal 46, XX karyotype (Fig. 2) and telomerase (Fig. 3A) activity. These three ICM-derived cell lines also expressed *Nanog*, *Oct3/4*, *Sox2*, *gp130*, *mCG*, *HEB*, and *Bex1/Rex3* mRNA and low levels of *FoxD3* and *Nestin* mRNA (Fig. 4A). Conversely, *LIFR* mRNA was not detected by RT-PCR. All three lines showed identical expression patterns of the genes. Therefore, we believe that these cells are CMESCs. To compare the gene expression patterns of fresh ICMs and the ICM-derived cell lines, RT-PCR analysis was conducted using fresh ICMs. As a result, the expression of *Nanog*, *Oct3/4*, and *Sox2* mRNA was

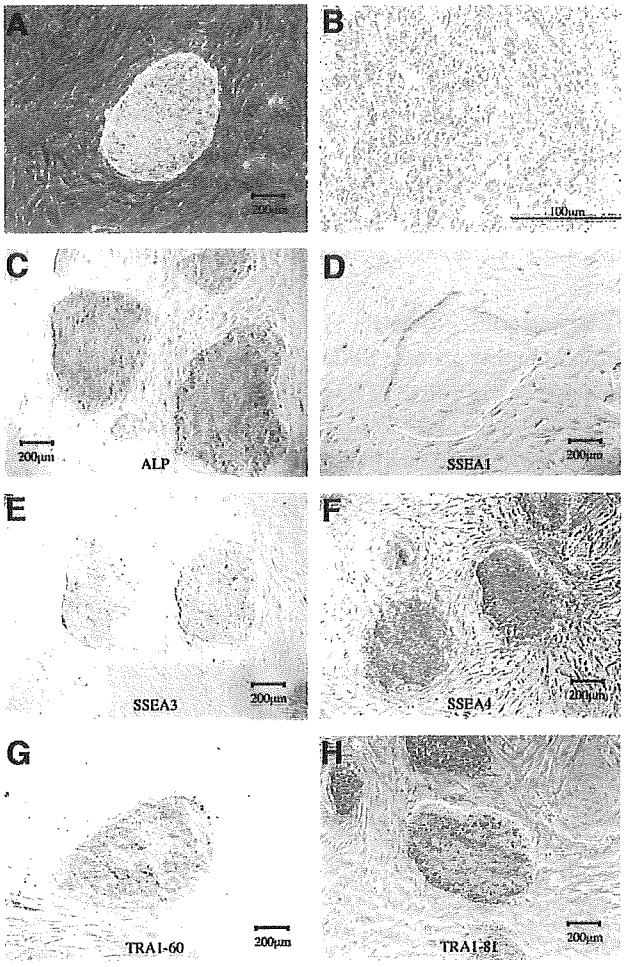

Figure 1. Expression of alkaline phosphatase and cell surface markers on CMESCs. Unstained CMESCs (**A, B**), cells stained for ALP (**C**), SSEA-1 (**D**), SSEA-3 (**E**), SSEA-4 (**F**), TRA-1-60 (**G**), and TRA-1-81 (**H**). Abbreviations: ALP, alkaline phosphatase; CMESC, common marmoset embryonic stem cell; SSEA, stage-specific embryonic antigen.

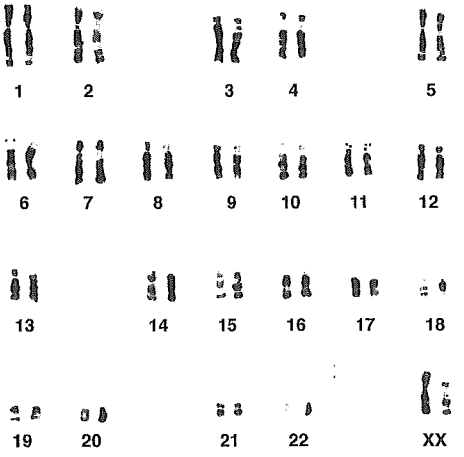

Figure 2. Karyotype analysis of CMESCs. The results for CIEA-CMESC #20 are shown. All three cell lines show the normal 46, XX karyotype after more than 6 months of culture. Abbreviations: CIEA, Central Institute for Experimental Animals; CMESC, common marmoset embryonic stem cell.

observed, whereas *FoxD3* and *Nestin* mRNA was not detected in fresh ICMs (Fig. 4B).

All three CMESC lines were examined for *MHC-DRB1* genotypes using PCR-based single strand conformation polymorphism (SSCP) methods. As shown in Figure 3B, the three CMESC lines were confirmed, based on different SSCP patterns, as having been established independently. Of these three CMESC lines, nos. 30 and 40 were derived from the same parents.

Differentiation Potency

Similar to other primate ESCs, CMESCs differentiate spontaneously during culturing on MEF feeder layer. However, the complete differentiation of CMESCs was suppressed by some growth factors or inhibitory factors from MEF feeder layer. To estimate the degree of differentiation, 50 CMESC clusters were seeded onto MEF feeder layer. As a result, 22%–74% ($n = 6$) of

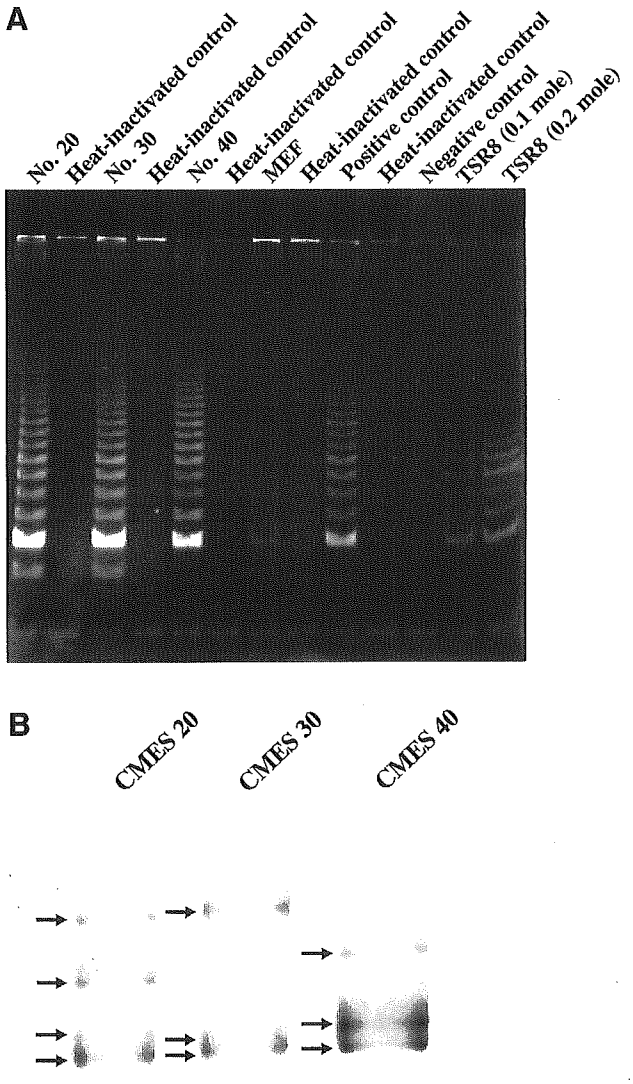

Figure 3. (A): Telomerase activities of CMESC lines. All three CMESC lines show high telomerase activity. On the other hand, MEF feeder layer does not show telomerase activity. **(B):** SSCP analysis of CMESCs for the *MHC-DRB1* gene. The results of SSCP indicate that all three lines were derived independently. Abbreviations: CMESC, common marmoset embryonic stem cell; MEF, mouse embryonic fibroblast; SSCP, single strand conformation polymorphism.

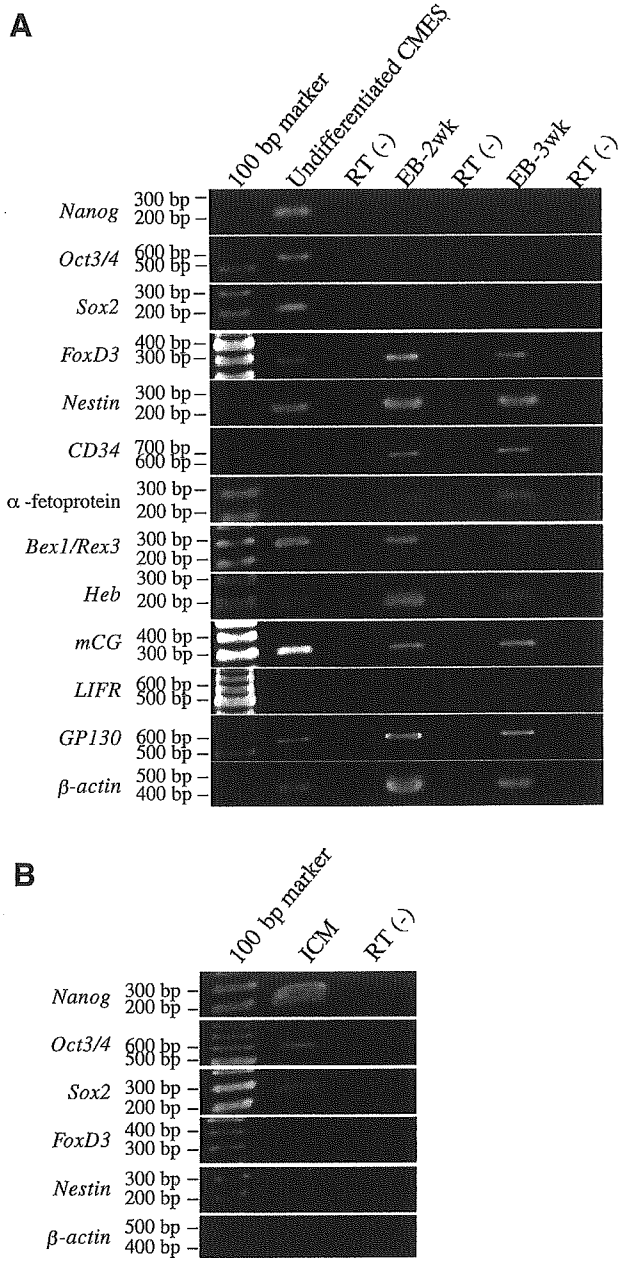

Figure 4. (A): RT-PCR analysis of CMESCs and EBs. Undifferentiated CMESCs expressed the *Nanog*, *Oct3/4*, *Sox2*, *FoxD3*, *Bex1/Rex3*, *Heb* and *mCG*, *GP130*, and low level of *Nestin* genes. Two-week cultures of EBs display expression of *Nestin* and *CD34*. Three-week cultures of EBs show expression of *Nestin*, *CD34*, and α-fetoprotein. *Oct3/4* and *Nanog* gene expression is shut down in the EBs. **(B):** RT-PCR analysis of fresh ICMs. ICMs expressed the *Nanog*, *Oct3/4*, and *Sox2* genes. Expression of *FoxD3* and *Nestin* was not detected. Abbreviations: CMESC, common marmoset embryonic stem cell; EB, embryoid body; ICM, inner cell mass; RT-PCR, reverse transcription–polymerase chain reaction.

the colonies (average 42.6%) were morphologically undifferentiated ESCs (data not shown). However, the differentiation rate of each cell was unclear because CMESCs need to be cell clusters to maintain undifferentiated status.

To assess the spontaneous differentiation potency of CMESCs, the formation of EBs and teratomas was examined. The suspension cultures of all three CMESC lines formed EBs (Figs. 5A, 5B). Simple EBs formed several days after the start of the suspension culture, and cystic EBs formed within 2 weeks. These EBs expressed mRNA for the *Nestin*, *CD34*, and α-fetoprotein genes, which are marker genes for the three germ layers, and *mCG*, *Bex1/Rex3*, and *Heb*, which are marker genes for trophectoderm (Fig. 4A). Furthermore, expression of *LIFR* and *gp130* was observed. However, *Nanog*, *Oct3/4*, and *Sox2* gene expression was shut off after 2 weeks of EB culture. In contrast, the expression level of *FoxD3* in EBs was greater than in undifferentiated CMESCs. To examine the differentiation potency in more detail, cells of CMESC 20 were injected subcutaneously into five immunodeficient NOG mice [11]. Eight weeks after injection, subcutaneous tumors were rescued from these mice and subjected to histological analysis. The tumor formation rate was 100% (5/5). The tumors were found to be teratomas that consisted of embryonic germ layers of ectodermal, mesodermal, and endodermal tissues (Figs. 6A–6M). Teratomas formed in all five NOG mice (100% teratoma formation rate). In the teratomas, the ectodermal tissue consisted of keratinized epidermis (Figs. 6B, 6G, and 7F) and neuronal cells (Fig. 6M); the mesodermal tissue was comprised of muscle (Figs. 6C, 6H) and blood vessels (Figs. 6I, 6J), and the endodermal tissue contained columnar epithelium (Figs. 6A, 6K, and 6L). Furthermore, cartilage-like tissue (Figs. 6A, 6D, and 6E) and adipose-like tissue (Fig. 6D) were also observed. These blood vessels were distinguished from murine blood vessels by immunohistochemical staining with human anti-CD31 antibody. Bronchus-like structures and gut-like structures were occasionally found in the teratomas (Figs. 6A, 6K, and 6L). Differentiation was confirmed by immunohistochemical analysis with several tissue-specific antibodies. As evidence for ESC differentiation into ectodermal cells, the GFAP-positive cells were observed as neuronal cells (Fig. 6M), and the keratinized epidermis-like structures in the teratomas expressed WSS keratin (Fig. 6G). The teratomas differentiated frequently into mesodermal tissues such as muscle, blood vessels, and cartilage. The muscle-like structure showed desmin expression, and CD31-positive cells were located in the hemangioendothelium of the blood vessel–like structures (Fig. 6J). The presence of the gut-like structures suggests endodermal differentiation. Alcian blue and periodic acid-Schiff (PAS) staining revealed mucus secretion from the columnar epithelium (Fig. 6L).

To investigate the in vitro differentiation potency of the CMESCs, the measurement of stromal cell–derived inducing activity (SDIA) was performed. After culture on PA6 cells for 20 days, extensive neurites appeared in the majority of the primate ESC colonies (67%, $n = 30$), which contained a large number of postmitotic neurons positive for class III β-tubulin (red; Fig. 7). SDIA has been reported to induce the production of tyrosine hydroxylase (TH)–positive dopaminergic neurons in mouse and

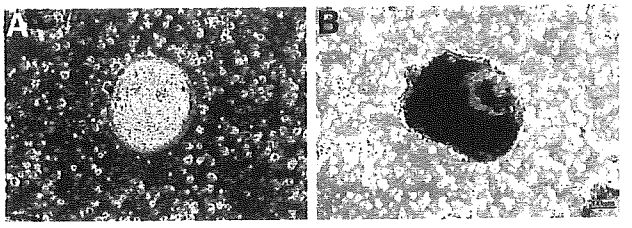

Figure 5. Spontaneous differentiation potency of CMESCs. A suspension culture of CMESCs shows the formation of EBs: **(A)** simple EB, **(B)** cystic EB. Abbreviations: CMESC, common marmoset embryonic stem cell; EB, embryoid body.

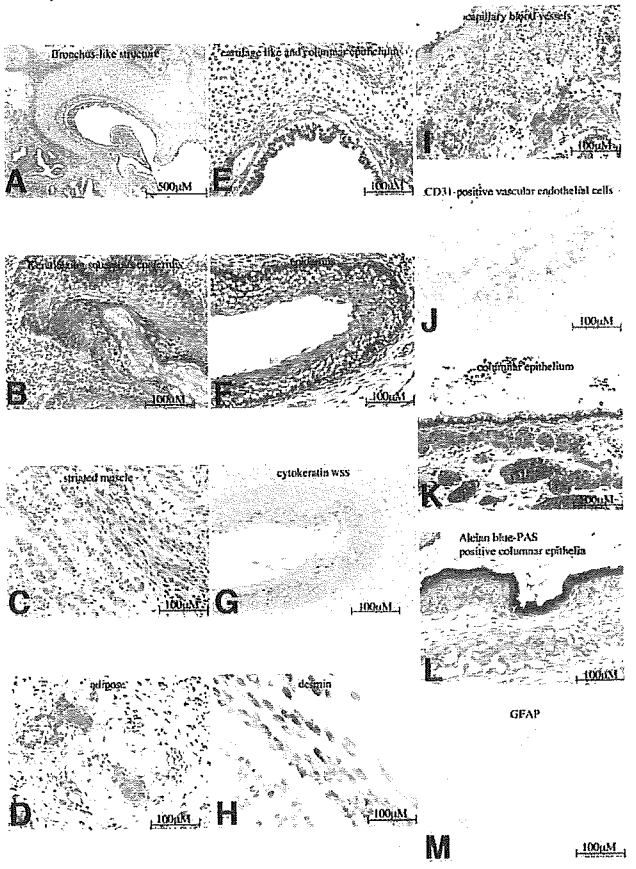

Figure 6. Differentiated CMESCs in teratomas and the expression of tissue-specific markers. **(A):** A bronchus-like structure that consists of columnar epithelium surrounded by cartilage-like tissue. **(B–M):** Keratinizing squamous epidermis **(B)**, striated muscle **(C)**, adipose-like tissue (high magnification) **(D)**, cartilage-like and columnar epithelium (high magnification) **(E)**, epidermis **(F)**, reactivity for cytokeratin WSS **(G)**, muscle-expressing desmin **(H)**, capillary blood vessels **(I)**, CD31-positive vascular endothelial cells **(J)**, columnar epithelium **(K)**, Alcian blue-PAS–positive columnar epithelia **(L)**, and GFAP-expressing neural cells **(M)**. Abbreviations: CMESC, common marmoset embryonic stem cell; GFAP, glial fibrillary acidic protein; PAS, periodic acid-Schiff; WSS, wide specific screening.

cynomolgus monkey ESCs and hESCs [17–19]. Therefore, we tested the marmoset cells for similar activities. After 2 weeks of induction, 14% of the class III β-tubulin–positive postmitotic neurons were TH-positive at the cellular level ($n = 50$). These cells were plated from trypsinized ESCs at passage. Most of the cells were derived from single cells, but only 15% of them expressed the TH protein. In the teratoma-like tumor induced by subcutaneous transplantation into NOG mice, some III β-tubulin–positive cells were found in colonies. Among III β-tublin–positive neurons, TH-positive neurons were found in 21% of them($n = 113$; data not shown).

To induce hematopoietic cells, EB formation was allowed to proceed in the cytokine-free medium, and CFU assays were performed. CFU-M (CFU-monocyte/macrophage) colonies were mainly observed under these conditions (Fig. 8A), and the main population of macrophages was confirmed microscopically using May-Giemsa staining of cytospun preparations (Fig. 8B).

Discussion

In this study, we have developed an embryo collection system that ensures a stable supply of common marmoset embryos for future production of transgenic or gene knockout marmosets. Our results show that marmoset ovulation is not disturbed, even after continuous administration of the PGF2α analogue cloprostenol. Thus, embryo collection from the same animal was carried out routinely, every 3 weeks, using cloprostenol administration. Using our embryo collection system, we recently established CMESC lines. In this study, we used a reported method of immunosurgery [9]. Although there was a high ICM isolation rate (85.7%) from blastocysts, the CMESC derivation rate was 18.3%, which is comparable to previous reports on other primate ESC lines, including 35.7% for human and 12.5% for cynomolgus monkey [14, 15]. The derivation rate of CMESC lines was considered to be dependent on the expansion procedure used for the cultured ICMs, including the in vitro developmental ability of embryos or the passage technique used for expanded ICMs.

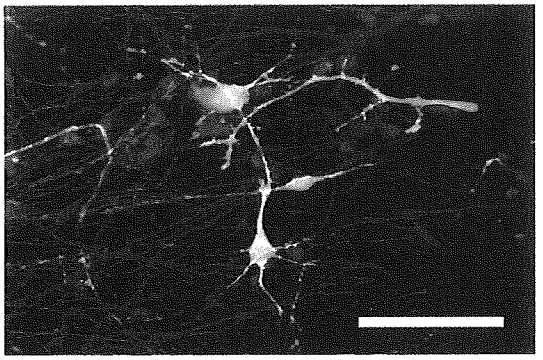

Figure 7. Neuronal cell differentiation of CMESCs in vitro. In vitro–differentiated ESCs using the SDIA method express TH protein and class III β-tubulin protein. Tyrosine hydroxylase: green; class III β-tubulin: red; Hoechst: blue. Scale bar = 80 mm. Abbreviations: CMESC, common marmoset embryonic stem cell; ESC, embryonic stem cell; SDIA, stromal cell–derived inducing activity.

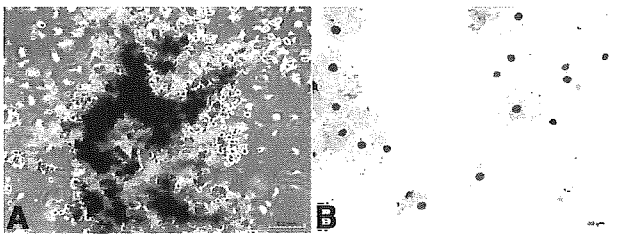

Figure 8. Hematopoietic CMESC differentiation in vivo. **(A):** CFU-M–like colonies predominate under these conditions. **(B):** May-Giemsa staining of colony-forming cells, confirming that the major population consists of macrophages. Abbreviations: CFU-M, colony-forming unit-monocyte/macrophage; CMESC, common marmoset embryonic stem cell.

The results of immunohistochemical analysis, enzymatic activity assays, RT-PCR analysis, and karyotype analysis show that the CMESC lines maintain their undifferentiated status. The RT-PCR results indicate that the gene expression patterns of undifferentiated CMESCs are similar to that of hESCs and different from those of mouse ESCs. In undifferentiated CMESCs, the expression patterns of *Oct3/4*, *Nanog*, *Sox2*, *mCG*, *HEB*, and *Bex1/REX3* gene mRNA were identical to hESCs or marmoset ESCs [6, 20]. In contrast, a very low level of *FoxD3* expression was observed in undifferentiated CMESCs. In fresh ICMs, the expression of *Nanog*, *Oct3/4*, and *Sox2* was observed, whereas that of *FoxD3* and *Nestin* was not. The presence of *Nanog*, *Oct3/4*, and *Sox2* mRNA expression in both fresh ICMs and CMESCs suggests that these genes are required to maintain stemness of cells in vitro and in vivo. Because *FoxD3* and *Nestin* were expressed at very low levels in undifferentiated CMESCs, it is possible that these genes in fresh ICMs are expressed under the detection level of our RT-PCR analysis. Another possibility is that the *FoxD3* and *Nestin* genes were amplified from spontaneously differentiated CMESCs in the cultured CMESCs. The latter possibility is supported by increased *FoxD3* gene expression in EBs. As the *FoxD3* gene expressed in murine undifferentiated ESCs [20], the different *FoxD3* expression patterns in primate and murine ESCs suggests that *FoxD3* plays a different role in respective ESCs. The expression of *mCG* and *Bex1/REX3* reflects the ability of CMESCs to differentiate into trophectodermal cells. These results match the ability of other primate ESCs to differentiate into trophectodermal cells.

The molecular mechanisms that maintain undifferentiated primate ESCs are largely unknown, and MEF feeder layer is essential to maintain undifferentiated primate ESCs. CMESCs also differentiated spontaneously on MEF feeder layer at low frequency. The expression of *gp130* and the absence of *LIFR* in CMESCs were identical to hESCs. These results indicate that maintaining undifferentiated CMESCs is not dependent on LIF signals. However, the expression of *gp130* suggested that other gp130-STAT3 signals, such as interleukin (IL)-6, oncostatin M,

or IL-11, play a role in CMESC proliferation or differentiation. The MEF feeder layer dependency of primate ESCs is considered one significant obstacle to using hESCs for stem therapy. Elucidation of the molecular mechanisms for the maintenance or development of MEF feeder layer–free culture systems of undifferentiated primate ESCs is one of the important themes of ESC research. Combined, these results suggest that the cellular characteristics and activities of CMESCs are similar to those of human and other primate ESCs [6, 12–16, 21, 22].

The spontaneous differentiation abilities of the CMESCs were verified by EB formation (Fig. 5) and teratoma formation (Fig. 6). RT-PCR analysis of EBs showed that the CMESCs differentiated into three germ layers in vitro. Furthermore, when the CMESCs were transplanted subcutaneously into immunodeficient NOG mice, teratomas that consisted of three-dimensional tissue structures were formed with high efficiency (100%). When SCID mice were used for the teratoma formation experiment, the teratoma formation rate was also 100% (two of two NOD/SCID mice, data not shown). Therefore, the formation of teratomas indicates that CMESCs have multipotent differentiation ability. The teratomas were also examined by immunohistochemistry, using several tissue-specific antibodies. The most frequently observed tissue type in the teratomas was mesodermal, which included cartilage (Figs. 6A, 6D, and 6E), muscle (Figs. 6C, 6H), and blood vessels (Fig. 6I). Although the frequency of endodermal tissue differentiation was lower than the frequencies of ectodermal and mesodermal tissue differentiation, endodermal tissue differentiation was clearly demonstrated with one of our CMESC lines (no. 20). Interestingly, Alcian blue and PAS staining of columnar epithelium showed the secretion of mucus from the cells, which indicates that CMESCs can differentiate into functional endodermal cells (Fig. 6L). Teratoma formation was not demonstrated for the marmoset ESC line (cj 11) established by Thomson et al. [6]. Both CMESC and cj 11 showed similar morphology and identical marker expression patterns. However, when we examined teratoma formation with a marmoset ESC line purchased from the WiCell Research Institute, Inc. (Madison, WI, http://www.wicell.org), we obtained fibrosarcomas, but no teratomas, in NOD/SCID mice (data not shown). The reasons for successful in vivo teratoma formation with our ESCs remain to be elucidated.

SDIA caused CMESC lines 20 and 40 to differentiate into TH-positive neurons in vitro (Fig. 7). In vitro differentiation into hematopoietic cells from EBs was measured in colony assays. Although other types of hematopoietic colonies were not seen in all experiments ($n > 7$), other conditions, such as gene-transfer methods, make it possible to induce various hematopoietic colonies from CMESCs (Kurita et al., personal communication), which suggests that CMESCs have the ability to differentiate into multiple hematopoietic lineages. These results support our finding that CMESCs have the capacity to differentiate into functional cells both in vitro and in vivo. Therefore, CMESCs can be used in preclinical studies aimed at developing regenerative medicines.

In this study, the teratoma formation and in vitro differentiation experiments show the strong differentiating potency of our CMESC lines; in addition, this is the first report to demonstrate the pluripotency of CMESCs. Our pluripotent CMESC lines should be very useful in establishing a preclinical animal model system for predicting the safety and efficacy of regenerative therapies using hESCs. Chimerism and the germ line transmission ability of CMESCs are not yet known. The mechanisms of the germ line transmission of ESCs are unknown, and in primates and other mammals, except mice, germ line transmission of ESCs has not been reported. Therefore, it is possible that germ line transmission of CMESCs will not occur in chimeras. If CMESCs do not transmit into the germ line, somatic cell nuclear transfer from the chimera or gametogenesis from CMESCs is one way to solve the problem [23–25].

Recently, various types of cells differentiated from hESCs or nonhuman ESCs have been reported [18, 26–36]. For example, hematopoietic cells, dopaminergic neurons, and insulin-producing cells have been generated from hESCs or primate ESCs. However, reports of transplantation of these differentiated ESCs into nonhuman primates are very rare [37]. There are various difficulties involved in using nonhuman primates as experimental animals. For example, rhesus or cynomolgus monkeys in which the ESC line has already been established are too expensive and cumbersome. Furthermore, immunological incompatibility between ESCs and animals may represent a significant obstacle to ESC transplantation. Taking this situation into consideration, the common marmoset has advantages, such as low cost and ease of maintenance. Importantly, marmosets are immunogenetically closed because they have been bred in large closed colonies. Thus, the common marmoset and CMESCs provide an excellent experimental model system for studies into the mechanism of cell differentiation, as well as for the development of regenerative therapies using hESCs.

Acknowledgments

We thank Dr. Sumiko Watanabe, Dr. Chieko Kai, and Dr. Ken-ichi Arai for very helpful advice and persistent support. This work was supported by grants from the Japan Society for the Promotion of Science and Research for the Future Program and partially by the Ministry of Education, Culture, Sports, Science, and Technology.

Disclosures

The authors indicate no potential conflicts of interest.

References

1 Lopata A, Summers PM, Hearn JP. Births following the transfer of cultured embryos obtained by in vitro and in vivo fertilization in the marmoset monkey (*Callithrix jacchus*). Fertil Steril 1988;50:503–509.

2 Summers PM, Shephard AM, Taylor CT et al. The effects of cryopreservation and transfer on embryonic development in the common marmoset monkey, *Callithrix jacchus*. J Reprod Fertil 1987;79:241–250.

3 Marshall VS, Kalishman J, Thomson JA. Nonsurgical embryo transfer in the common marmoset monkey. J Med Primatol 1997;26:241–247.

4 Hibino H, Tani K, Ikebuchi K et al. The common marmoset as a target preclinical primate model for cytokine and gene therapy studies. Blood 1999;93:2839–2848.

5 Mansfield K. Marmoset models commonly used in biomedical research. Comp Med 2003;53:383–392.

6 Thomson JA, Kalishman J, Golos TG et al. Pluripotent cell lines derived from common marmoset (*Callithrix jacchus*) blastocysts. Biol Reprod 1996;55:254–259.

7 Summers PM, Wennink CJ, Hodges JK. Cloprostenol-induced luteolysis in the marmoset monkey (*Callithrix jacchus*). J Reprod Fertil 1985;73:133–138.

8 Harlow CR, Gems S, Hearn JP et al. The relationship between plasma progesterone and the timing of ovulation and early embryonic development in the marmoset monkey (*Callithrix jacchus*). J Zool 1983;201:273–282.

9 Solter D, Knowles BB. Immunosurgery of mouse blastocyst. Proc Natl Acad Sci U S A 1975;72:5099–5102.

10 Wu MS, Tani K, Sugiyama H et al. MHC (major histocompatibility complex)-DRB genes and polymorphisms in common marmoset. J Mol Evol 2000;51:214–222.

11 Ito M, Hiramatsu H, Kobayashi K et al. NOD/SCID/gamma(c)(null) mouse: an excellent recipient mouse model for engraftment of human cells. Blood 2002;100:3175–3182.

12 Thomson JA, Kalishman J, Golos TG et al. Isolation of a primate embryonic stem cell line. Proc Natl Acad Sci U S A 1995;92:7844–7848.

13 Reubinoff BE, Pera MF, Fong CY et al. Embryonic stem cell lines from human blastocysts: somatic differentiation in vitro. Nat Biotechnol 2000;18:399–404.

14 Suemori H, Tada T, Torii R et al. Establishment of embryonic stem cell lines from cynomolgus monkey blastocysts produced by IVF or ICSI. Dev Dyn 2001;222:273–279.

15 Thomson JA, Itskovitz-Eldor J, Shapiro SS et al. Embryonic stem cell lines derived from human blastocysts. Science 1998;282:1145–1147.

16 Mitalipova M, Calhoun J, Shin S et al. Human embryonic stem cell lines derived from discarded embryos. STEM CELLS 2003;21:521–526.

17 Kawasaki H, Mizuseki K, Nishikawa S et al. Induction of midbrain dopaminergic neurons from ES cells by stromal cell-derived inducing activity. Neuron 2000;28:31–40.

18 Kawasaki H, Suemori H, Mizuseki K et al. Generation of dopaminergic neurons and pigmented epithelia from primate ES cells by stromal cell-derived inducing activity. Proc Natl Acad Sci U S A 2002;99:1580–1585.

19 Perrier AL, Tabar V, Barberi T et al. Derivation of midbrain dopamine neurons from human embryonic stem cells. Proc Natl Acad Sci U S A 2004;101:12543–12548.

20 Ginis I, Luo Y, Miura T et al. Differences between human and mouse embryonic stem cells. Dev Biol 2004;269:360–380.

21 Stojkovic M, Lako M, Stojkovic P et al. Derivation of human embryonic stem cells from day-8 blastocysts recovered after three-step in vitro culture. STEM CELLS 2004;22:790–797.

22 Stojkovic M, Lako M, Strachan T et al. Derivation, growth and applications of human embryonic stem cells. Reproduction 2004;128:259–267.

23 Toyooka Y, Tsunekawa N, Akasu R et al. Embryonic stem cells can form germ cells in vitro. Proc Natl Acad Sci U S A 2003;100:11457–11462.

24 Hubner K, Fuhrmann G, Christenson LK et al. Derivation of oocytes from mouse embryonic stem cells. Science 2003;300:1251–1256.

25 Simerly C, Navara C, Hyun SH et al. Embryogenesis and blastocyst development after somatic cell nuclear transfer in nonhuman primates: overcoming defects caused by meiotic spindle extraction. Dev Biol 2004;276:237–252.

26 Assady S, Maor G, Amit M et al. Insulin production by human embryonic stem cells. Diabetes 2001;50:1691–1697.

27 Schuldiner M, Eiges R, Eden A et al. Induced neuronal differentiation of human embryonic stem cells. Brain Res 2001;913:201–205.

28 Kaufman DS, Hanson ET, Lewis RL et al. Hematopoietic colony-forming cells derived from human embryonic stem cells. Proc Natl Acad Sci U S A 2001;98:10716–10721.

29 Kehat I, Kenyagin-Karsenti D, Snir M et al. Human embryonic stem cells can differentiate into myocytes with structural and functional properties of cardiomyocytes. J Clin Invest 2001;108:407–414.

30 Umeda K, Heike T, Yoshimoto M et al. Development of primitive and definitive hematopoiesis from nonhuman primate embryonic stem cells in vitro. Development 2004;131:1869–1879.

31 Haruta M, Sasai Y, Kawasaki H et al. In vitro and in vivo characterization of pigment epithelial cells differentiated from primate embryonic stem cells. Invest Ophthalmol Vis Sci 2004;45:1020–1025.

32 Mizuseki K, Sakamoto T, Watanabe K et al. Generation of neural crest-derived peripheral neurons and floor plate cells from mouse and primate embryonic stem cells. Proc Natl Acad Sci U S A 2003;100:5828–5833.

33 Kuo HC, Pau KY, Yeoman RR et al. Differentiation of monkey embryonic stem cells into neural lineages. Biol Reprod 2003;68:1727–1735.

34 Calhoun JD, Lambert NA, Mitalipova MM et al. Differentiation of rhesus embryonic stem cells to neural progenitors and neurons. Biochem Biophys Res Commun 2003;306:191–197.

35 Lang KJ, Rathjen J, Vassilieva S et al. Differentiation of embryonic stem cells to a neural fate: a route to re-building the nervous system? J Neurosci Res 2004;76:184–192.

36 Li F, Lu S, Vida L et al. Bone morphogenetic protein 4 induces efficient hematopoietic differentiation of rhesus monkey embryonic stem cells in vitro. Blood 2001;98:335–342.

37 Nara Y, Muramatsu S, Nakano I. ES cell therapy for Parkinson's disease. Nippon Rinsho 2004;62:1643–1647.

A Novel Role of CD30/CD30 Ligand Signaling in the Generation of Long-Lived Memory CD8$^+$ T Cells[1]

Hitoshi Nishimura,* Toshiki Yajima,* Hiromi Muta,† Eckhard R. Podack,‡ Kenzaburo Tani,† and Yasunobu Yoshikai[2]*

Memory CD8$^+$ T cells can be divided into two subsets, central memory (T_{CM}) and effector memory (T_{EM}) CD8$^+$ T cells. We found that CD30, a member of the TNFR-associated factor (TRAF)-linked TNFR superfamily, signaling is involved in differentiation of long-lived CD8$^+$ T_{CM} cells following *Listeria monocytogenes* infection. Although CD8$^+$ T_{EM} cells transiently accumulated in the nonlymphoid tissues of CD30 ligand (CD153$^{-/-}$) mice after infection, long-lived memory CD8$^+$ T_{CM} cells were poorly generated in these mice. CCR7 mRNA expression was down-regulated in CD8$^+$ T cells of the spleen of CD153$^{-/-}$ mice in vivo and the expression was up-regulated in CD8$^+$ T_{EM} cells by anti-CD30 mAb cross-linking in vitro. These results suggest that CD30/CD30 ligand signaling plays an important role in the generation of long-lived memory CD8$^+$ T cells at least partly by triggering homing receptors for T_{CM} cells. *The Journal of Immunology,* **2005, 175: 4627–4634.**

Generation and maintenance of long-lived CD8$^+$ T cell memory are important goals of vaccination because they can provide protection against reinfection of many pathogens, including intracellular bacteria (1). Immune response against the pathogens depends on the ability of lymphocytes to migrate to appropriate places within the body to find their cognate Ags (2). Memory CD8$^+$ T cells have been divided into two subsets based on their anatomical location, expression of cell surface markers, and effector functions (3). Memory T cells expressing homing receptors such as CD62 ligand (CD62L)[3] and CCR7, which allow efficient homing to lymph nodes (LNs), are termed central memory (T_{CM}) cells, whereas memory T cells lacking these LN-homing receptors, which are located in nonlymphoid tissues, are termed effector memory (T_{EM}) cells. T_{CM} cells have been reported to produce few effector molecules but to have homeostatic proliferative capacity in response to IL-15 (4, 5). In contrast, T_{EM} cells are thought to facilitate their entry into infected tissues expressing cognate effector molecules for these receptors (4, 5). It is suggested that T_{CM} and T_{EM} cells do not necessarily represent distinct subsets and that they are part of a continuum in a linear naive effector-T_{EM}-T_{CM} differentiation pathway (4). In contrast, there is some evidence that T_{CM} and T_{EM} cells might be generated differentially during primary immune response depending on the conditions of activation (5). However, very little is known about signaling that regulates the differentiation pathway of these memory T cells.

Signaling via the TNFR superfamily regulates the fate of activated T cells (6). Members of the TNFR superfamily such as Fas and TNFR type I, which contain a death domain in the cytoplasmic tail, are responsible for activation-induced T cell death (7), whereas members having no death domain such as CD40 and CD70 play a key role in effective T cell immunity (6). For example, generation of memory CD8$^+$ T cells displaying an enhanced capacity for cell division and cytokine secretion requires CD40L expression by CD4$^+$ T cells (8–11). CD30, a member of the TNFR superfamily, is expressed by activated or memory CD8$^+$ T cells but not by resting B or T cells (12–14). A CD30 ligand (CD30L, CD153) is a 40-kDa type II membrane-associated glycoprotein belonging to the TNF family (15). CD153 is expressed on macrophages, dendritic cells, and B cells (6, 14–16). Little is known about the role of CD30/CD30L signaling in generation of memory CD8$^+$ T cells, although there are several lines of evidence showing that the signaling regulates peripheral T cell response through controlling T cell survival and down-regulation of cytolytic capacity (17–22).

We previously reported that gene expression of CCR7 is up-regulated by CD30 stimulation in the human YT lymphoma cell line (23, 24). This raises the possibility that CD30/CD30L signaling plays an important role in differentiation of memory T cell subsets following Ag exposure. In the present study, we found with CD153$^{-/-}$ mice that CD30/CD30L signaling is involved in differentiation of CD8$^+$ T_{CM} cells following exposure to a microbe.

Materials and Methods

Mice

Age- and sex-matched BALB/c mice were obtained from Charles River Breeding Laboratories. The generation and preliminary characterization of CD153$^{-/-}$ mice were previously described (24). All mice were maintained under specific pathogen-free conditions and were offered food and water ad libitum. All mice were used at 6–8 wk of age.

*Division of Host Defense, Center for Prevention of Infectious Disease, and †Division of Molecular Genetics, Medical Institute of Bioregulation, Kyushu University, Fukuoka, Japan; and ‡Department of Microbiology and Immunology, University of Miami, Miami, FL 33101

Received for publication August 10, 2004. Accepted for publication July 14, 2005.

The costs of publication of this article were defrayed in part by the payment of page charges. This article must therefore be hereby marked *advertisement* in accordance with 18 U.S.C. Section 1734 solely to indicate this fact.

[1] This work was supported in part by a Grant-in Aid for Scientific Research on Priority Areas, Japan Society for the Promotion of Science, and by grants from the Japanese Ministry of Education, Science and Culture (to Y.Y.), Yakult Bioscience Foundation (to Y.Y.), Uehara Memorial Foundation (to Y.Y.), Nakamura Jishirou Foundation (to H.N.), Kurozumi Medical Foundation (to H.N.), and Kanzawa Medical Research Foundation (to H.N.).

[2] Address correspondence and reprint requests to Dr. Yasunobu Yoshikai, Division of Host Defense, Center for Prevention of Infectious Disease, Medical Institute of Bioregulation, Kyushu University, Fukuoka 812-8582, Japan. E-mail address: yoshikai@bioreg.kyushu-u.ac.jp

[3] Abbreviations used in this paper: CD62L, CD62 ligand; LN, lymph node; T_{CM}, central memory T cell; T_{EM}, effector memory T cell; Tc, T cytotoxic cell; LLO, listeriolysin O; CD30L, CD30 ligand; TRAF, TNFR-associated factor.

0022-1767/05/$02.00

Microorganism

Listeria monocytogenes strain EGD was used in all experiments. Bacterial virulence was maintained by serial passages in BALB/c mice. Mice were inoculated i.p. with various doses of viable *L. monocytogenes* in 0.2 ml of PBS on day 0. The spleen and liver were removed from each mouse and separately placed on trypto-soya agar plates, and colonies were counted after incubation for 24 h at 37°C.

Abs and reagents

FITC-conjugated anti-CD44 (IM7), anti-CD69 (H1.2F3), and anti-IFN-γ (XMG1.2); PE-conjugated anti-CD8α (53-6.7), anti-CD44 (IM7), and anti-CD62L (MEL-14); and CyChrome-conjugated anti-CD8α (53-6.7) and anti-CD4 (RM4-5) were purchased from BD Pharmingen. CyChrome and allophycocyanin-conjugated streptavidin were also obtained from BD Pharmingen. CFSE was purchased from Molecular Probes.

Generation of H2-K^d tetramers

MHC-peptide tetramers for staining of epitope-specific cells were generated as previously described (25, 26). Briefly, purified H chain and β_2-microglobulin were dissolved in 8 M urea and diluted in a refolding buffer containing a high concentration of synthetic peptide listeriolysin O (LLO_{91-99}) (27) or JAK1 self-peptide (28) to generate monomeric soluble H2-K^d-peptide complexes. Biotinylation and tetramerization of the heterodimer were performed as described by Altman et al. (25). The monomeric complexes were tetramerized by the addition of PE-labeled streptavidin (BD Pharmingen) at a molar ratio of 4:1.

Flow cytometry analysis

The cells were incubated with saturating amounts of FITC-, PE-, CyChrome-, and biotin-conjugated mAbs for 30 min at 4°C. To detect biotin-conjugated mAbs, cells were stained with CyChrome- or allophycocyanin-conjugated streptavidin. For staining of epitope-specific CD8$^+$ T cells using the tetrameric H2-K^d-peptide complex, cells were incubated at 4°C for 20 min in unconjugated-streptavidin (0.5 mg/ml; Sigma-Aldrich) and Fc block (2.4G2), followed by triple staining with FITC-CD44, CyChrome-CD8α, and PE-conjugated tetrameric H2-K^d-peptide complex (0.2–0.3 mg/ml) for 30 min at 4°C. The cells were analyzed using an FACSCalibur flow cytometer (BD Biosciences).

Analysis of intracellular cytokine synthesis

Spleen cells were harvested from infected mice, washed, and suspended at 10^6 cells/ml in complete culture medium and then incubated for 4 h at 37°C in the presence of 10 mg/ml brefeldin A (Sigma-Aldrich) and 5 μg/ml LLO_{91-99} peptide. These cells were harvested, washed, and incubated for 30 min at 4°C with PE-conjugated anti-CD44 mAb and CyChrome-conjugated CD8 mAb. After surface staining, cells were subjected to intracellular cytokine staining using a Fast Immune Cytokine System according to the instructions of the manufacturer (BD Biosciences). The cells were washed and fixed in 100 μl of FACS lysing solution (BD Biosciences) for 10 min at room temperature and were then washed again, resuspended in 500 μl of FACS permeabilizing solution (BD Biosciences), and incubated for 10 min at room temperature. After washing, the cells were stained with FITC-conjugated IFN-γ mAb or FITC-conjugated isotype control rat IgG (BD Pharmingen) for 30 min at room temperature, and the fluorescence of the cells was analyzed using a flow cytometer.

Cell culture

Magnetic bead-separated CD8$^+$ T cells (95% pure) from LN were cultured in 200 μl of complete culture medium in a 96-well flat-bottom plate (BD Biosciences) at density of 5×10^5 cells/well with indicated concentrations of LLO_{91-99} peptide. To estimate IFN-γ production, the supernatant was collected at 48 h. The IFN-γ production in the supernatants was assayed using DuoSet ELISA development system (Genzyme). Proliferative activity of CD8$^+$ T cells was assessed by incorporation of [^{3}H]thymidine. The cells were pulsed with [^{3}H]thymidine 6 h before harvesting. [^{3}H]Thymidine incorporation was then determined by liquid scintillation counting.

RT-PCR

Nylon wool-enriched spleen T cells were incubated with appropriate dilutions of FITC-conjugated anti-I-A^d, IgM, and biotinylated anti-DX-5, anti-CD11c, and anti-$\gamma\delta$ TCR mAbs, and washed twice in HBSS. The cells were then incubated with anti-FITC microbeads, streptavidin microbeads, and anti-CD4 mAb microbeads for 15 min at 4°C. CD8$^+$ T cells were enriched to >90% by negative selection using LD-positive depletion columns (Miltenyi Biotec). T_{EM} (CD62L$^-$CD44$^+$CD8$^+$) cells were negatively separated with anti-CD62L mAb microbeads and anti-CD4 mAb microbeads from nylon wool-enriched spleen T cells (>95% purity). Total RNA was isolated from CD8$^+$ T cells and from CD62L$^-$CD44$^+$CD8$^+$ T cells of CD153$^{-/-}$ mice and control mice with TRIzol reagent (Invitrogen Life Technologies). The first-strand cDNA synthesized from the total RNA was amplified using 10 pmol of each primer specific for murine rRNA or chemokine receptors. cDNA encoding chemokine receptors was analyzed by real-time PCR using a TaqMan PCR kit and an ABI PRISM 7000 sequence detector thermal cycler according to the protocol recommended by the manufacturer (Applied Biosystems).

In vivo cytotoxicity assay

Analysis of in vivo cytolytic activity was conducted basically according to the previously reported protocol (29, 30). BALB/c splenocytes were divided into two populations and labeled with either a high concentration (3 μM) or a low concentration (0.3 μM) of CFSE. Next, CSFE^{high} cells were pulsed with 10^{-6} M LLO_{91-99} for 1 h at 37°C in the dark, whereas CFSE^{low} cells remained nonpulsed. After washing, CFSE^{high} cells were mixed with equal numbers of CSFE^{low} cells, and a suspension of 2×10^7 of these cells was i.v. injected into each mouse. Spleens from recipients were obtained 15 h later for flow cytometric analysis to measure in vivo killing as indicated by loss of the CFSE^{high} Ag-pulsed population relative to the control CFSE^{low} population. Percentage of specific lysis was calculated according to the following formula: [1 − (ratio of unprimed cells/ratio of primed cells) × 100], in which the ratio of unprimed cells is the percentage of CFSE^{low} per CFSE^{high} cells remaining in noninfected recipients, and the ratio of primed cells is the percentage of CFSE^{high} cells remaining in infected recipients.

Statistical analysis

Data were analyzed by Student's t test, and Bonferroni correction was applied for multiple comparison. A value of $p < 0.05$ was considered statistically significant.

Results

CD153 is required for generation of long-lived memory CD8$^+$ T cells

We studied the kinetics of bacterial clearance and the expansion, contraction, and stable memory of Ag-specific CD8$^+$ T cells in CD153-deficient mice with a BALB/c background after i.p. inoculation with 1×10^5 CFU of *L. monocytogenes* strain EGD. We found that the numbers of bacteria increased to maximal levels on day 3 in the spleen and liver and thereafter cleared completely by day 10 after inoculation in both wild-type mice and CD153$^{-/-}$ mice. We also found that the bacteria were more rapidly eliminated in wild-type mice than in CD153$^{-/-}$ mice (data not shown). To directly follow the fate of the *L. monocytogenes* epitope-specific CD8$^+$ T cells in CD153$^{-/-}$ mice after i.p. inoculation with *L. monocytogenes*, we used intracellular IFN-γ staining in response to LLO_{91-99} peptide, the immunodominant epitope recognized by H-2K^d-restricted CD8$^+$ T cells (Fig. 1*A*), and tetrameric MHC molecule folding with the LLO_{91-99} peptide (Fig. 1*B*) for staining epitope-specific CD8$^+$ T cells. As shown in Fig. 1*A*, a significant number of CD8$^+$ T cells expressing high levels of CD44 in the spleen and peritoneal cavity were stained with intracellular IFN-γ in CD153$^{-/-}$ mice on day 7 after infection with *L. monocytogenes* at the induction stage of effector T cells, albeit at a lesser level of CD44 than that found in wild-type mice. However, the absolute number of LLO_{91-99}-specific CD8$^+$ T cells in the peritoneal cavity of CD153$^{-/-}$ mice was $3.1 \pm 0.3 \times 10^5$ cells in CD153$^{-/-}$ mice, comparable to that found in wild-type mice of $3.4 \pm 0.4 \times 10^5$ cells (Fig. 2). These results suggest that the generation of effector CD8$^+$ T cells normally occurs in CD153$^{-/-}$ mice following *Listeria* infection.

In contrast, the numbers of LLO_{91-99}-specific CD8$^+$ T cells were significantly higher in the peritoneal cavity on days 28 and 42